Assessing the influence of long-range transport of aerosols on the PM$_{2.5}$ chemical composition and concentration in the Aburrá Valley

Maria P. Velásquez-García[1,3,4], K. Santiago Hernández[2], James A. Vergara-Correa[1], Richard J. Pope[3,4], Miriam Gómez-Marín[1], and Angela M. Rendón[2]

[1]Grupo de Higiene y Gestión Ambiental , Politécnico Jaime Isaza Cadavid, Medellín, Colombia
[2]Grupo de Investigación en Ingeniería y Gestión Ambiental, Universidad de Antioquia, Medellín, Colombia
[3]School of Earth and Environment, University of Leeds, Leeds, UK
[4]National Centre for Earth Observation, University of Leeds, Leeds, UK

Correspondence: Maria P. Velásquez-García (eempvg@leeds.ac.uk)

Abstract. Assessing long-range transport (LRT) of pollutants recognizes that multiple sources of varying scale and location can impact air quality. In the Aburrá Valley, Colombia, and other cities in Northern South America, biomass burning (BB), dust, and volcanic degassing have been identified as sources of LRT of aerosols. However, the impact of these sources on air quality and their characterization have yet to be thoroughly studied. This work investigates the influence of these sources on the chemical composition of PM$_{2.5}$ during annual and intra-annual high-load aerosol events. We identified, tracked, and meteorologically characterized LRT events and evaluated their influence on PM$_{2.5}$ concentration and chemical composition. We ran a Positive Matrix Factorization (PMF) for each kind of event, identifying high contribution in organic carbon (OC1, OC2), F$^-$ and secondary aerosols trace SO$_4^{2-}$ and NO$_3^-$ for the BB events, crustal mineral along with Ti and Ca contribution for dust events and SO$_4^{2-}$, Na, Al and Ca for volcanic events. The increasing concentration of some ions and toxic heavy metals (Cr, Mn, Cd, and Ni) were also related to BB and volcanic degassing influence. During these LRT events, the BB fraction of PM$_{2.5}$ dominates by frequency and amount, averaging 11.14 $\mu g/m^3$ (38%). On average, dust and volcanic degassing contribute 6.77 $\mu g/m^3$ (34%) and 6.46 $\mu g/m^3$ (30%) of the concentrations. Of the three, dust events showed fewer affected days. The study highlighted hotspot zones such as the Orinoco and Middle Magdalena Valley for BB aerosols, the Caribbean for dust, and the Nevado del Ruíz volcano for volcanic aerosols. This study gives insights for future chemical transport modeling studies in the region and supports strategies to manage internal and external pollution sources and effects for the Aburrá Valley and the region.

1 Introduction

Long-range transport (LRT) of aerosols influences the chemical composition of air over thousands of kilometers (Kaneyasu et al., 2014; Wang et al., 2015) and plays a crucial role in the biogeochemical cycle of some components, such as dust and

biomass aerosols, which distribute iron and phosphorus across the oceans and continents (Okin et al., 2004; Boyd and Ellwood, 2010). Furthermore, aerosols interact with solar radiation, influencing cloud formation and light scattering (absorbance) with a cooling (warming) effect on the planet (Choobari et al., 2014). In particular, dust and black carbon can contribute to albedo reduction and accelerate melting in snow-covered zones, significantly affecting climate worldwide (Kaspari et al., 2014).

25   LRT of aerosols also increases human health risks, particularly in urban areas with high local emissions. Above all, fine aerosols, represented by $PM_{2.5}$ (particulate matter with a diameter less than 2.5 μm), penetrate deeply into the human body and trigger cerebrovascular and heart diseases, lung cancer and obstruction, and respiratory infections (Xie et al., 2021; Lippmann et al., 2013). Indeed, LRT of $PM_{2.5}$ enlarges overall concentration to more dangerous levels and can increase specific components with particular effects on human health. For instance, carbonaceous dominant particles are assumed to be more

30   toxic than crustal components (Tuomisto et al., 2008). Increased OC (organic carbon) and EC (elemental carbon) associated with biomass burning episodes drive cardiovascular diseases (Hwang et al., 2017).

The accountability of $PM_{2.5}$ from LRT has urged cooperation between cities and countries to identify and control pollution increases and population vulnerability. For decades, in Europe and Asia, LRT of pollutants has been recognized as a significant factor for air pollution (Kulshrestha et al., 2014), and accounted into policy plans. For instance, the Task Force on Hemispheric

35   Transport of Air Pollution (TF HTAP) is a collaboration led by the European Union and the United States that targets intercontinental and north-hemisphere transport of PM and O_3, acknowledging their influence in meeting air quality goals (UN, 2010). The collaboration has contributed to identifying regional sources, tracking, and basing more effective emission reduction strategies (Liang et al., 2018; Zhao et al., 2021; Dong et al., 2018). On a smaller scale, Hong Kong/Guangdong Cooperation addresses transboundary air pollution in the Pearl River Delta Region (Zhong et al., 2013). The collaboration task consists of

40   monitoring pollution level changes, evaluating the effectiveness of control measures, and providing training to stakeholders.

In Northern South America (NSA), LRT of pollutants is a more recently recognized public problem, and regional cooperation is gaining importance and momentum. Three primary kinds of LRT of aerosols have been identified in the region: biomass burning, desert dust, and volcanic emissions. Although for South America, biomass burning around the Amazon basin is one of the primary sources of aerosols (Ballesteros-González et al., 2020), atmospheric circulation patterns and substantial

45   precipitation (i.e. aerosol wet deposition) means there is limited LTR of aerosols towards Colombia (Hamburger et al., 2013). So, transboundary emissions from open fires in the Orinoco basin and the Caribbean are significant drivers of intra-annual periods of hazardous air quality for Colombian cities such as Bogotá, Medellín, Arauca, Yopal, Bucaramanga and Villavicencio (Mendez-Espinosa et al., 2019; Henao et al., 2021; Hernandez et al., 2019; Rodríguez-Gómez et al., 2022) and on Pico Espejo in Venezuela (Hamburger et al., 2013).

50   Likewise, LRT of dust has also been reported in NSA, mainly produced from Sahara and Sahel deserts (Prospero et al., 2020). These primarily affect the Caribbean region, as reported in islands as Barbados, Guadalupe, Virginia, and Tobago Island, and the continental land with the Cayenne (French Guiana) (Prospero et al., 2014; Kumar et al., 2014). African dust effects have also been reported in Colombia, with the analysis of high particle loads on June 2014 and 2020 (Bolaño-Ortiz et al., 2023a; Mendez Espinosa et al., 2018; Bedoya et al., 2016). Notably, the LRT of African dust in June 2014 covered 95% of the country

55   (dust concentrations $> 90 kgkm^{-2}$) (Mendez Espinosa et al., 2018). Few long-term assessments have also been done in the Caribbean and Andean regions (Bolaño-Ortiz et al., 2023b; Arregocés et al., 2023).

Volcanic activities (eruption and degassing) also play a crucial role in the LRT of pollutants in NSA and are part of the natural ecosystem in the region since it belongs to the Andean volcanic belt. Few studies have been conducted on air quality, which has mainly focussed on the Sangay volcano in Ecuador and Nevado del Ruíz in Colombia (Casallas et al., 2024; Moran-Zuloaga

60   et al., 2023). These studies track $PM_{2.5}$ and Sulfur dioxide(SO_2) in the air and road particles from the volcanoes (Casallas et al., 2024; Cuesta-Mosquera et al., 2020; Trejos et al., 2021). The degassing activities for the Nevado del Ruíz have been especially highlighted for their magnitude and frequency (Carn et al., 2016).

In Colombia, the Aburrá Valley (AV) has made substantial progress in monitoring and identifying agents of the state of air quality in the territory, managing to report significant affectation driven by external sources (SIATA, 2021). In the territory,

65   as on the national scale, open fire emissions have been intensely investigated in the last few years (Ballesteros-González et al., 2020; Mendez-Espinosa et al., 2019; Henao et al., 2021). In contrast, dust and volcanic aerosols studies have been limited to episodic high-pollution events (Mendez Espinosa et al., 2018) and do not provide comprehensive information on the sources' influence and the aerosols transport (Liu et al., 2022). Even though, for the three kinds of emissions sources, there are still significant gaps in understanding the representative influence on regional air quality throughout the year and

70   their impact on aerosol composition, particularly for dust and volcanic aerosols, which are frequently overlooked due to their uncontrolled nature (Woo et al., 2020; Pouliot et al., 2012). To the AV, obtaining the annual representation of the LRT of aerosols would contribute to the characterization of concentrations at local and national scales. It enables decision-makers to develop cooperative and effective projects to manage the risk of air pollution involving natural sources (Gómez Peláez et al., 2020; Jiao et al., 2021). Furthermore, advances in the characterization of the chemical composition of air give rise to strategies

75   to reduce the exposure of the population to high concentrations of certain species such as toxic heavy metals and carbonaceous matter (Gómez Peláez et al., 2020; Briffa et al., 2020; Allajbeu et al., 2017).

This study aims to analyze the impact of LRT of biomass burning (BB-LRT), dust (Dust-LRT), and volcanic aerosols (Volcanic-LRT) on $PM_{2.5}$ concentrations and chemical composition through year-frequent high aerosol load events in the AV. We characterize meteorologically favorable conditions for transport to the valley and involve information from one of the

80   largest registered $PM_{2.5}$ chemical characterization campaigns conducted in the territory (April 2019 to October 2022), as well as in-situ $PM_{2.5}$ measurements and satellite-based products. We identify representative events, analyze atmospheric transport, and highlight potential sources. Finally, we evaluate the impact of these sources on ground-level $PM_{2.5}$ concentrations and chemical composition in the AV.

2   Data and Methods

85   ### 2.1   Study region

The AV, illustrated in Fig. 1b, is a 1.152 km² natural river basin located in the northeast of Colombia (see Fig. 1a). The territory contains ten cities, with Medellín as the largest city. The AV is in the central mountain range of the Colombian Andes, and
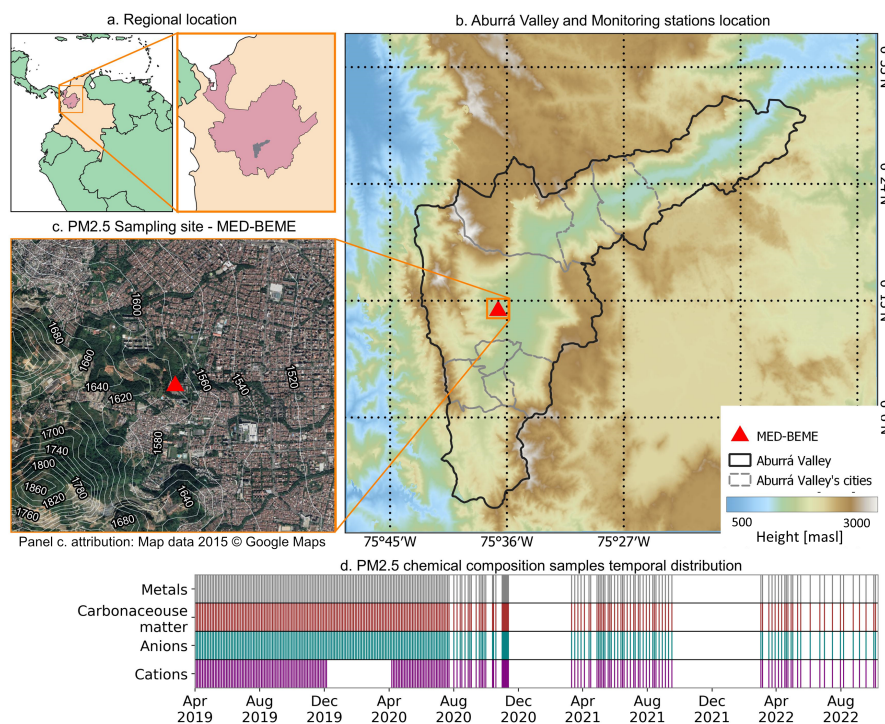
Figure 1. a. Regional location of the AV, b. Geomorphology of the AV and the distribution of the ten municipalities in black lines; c. Location of the $PM_{2.5}$ chemical sampling campaign station (MED-BEME), represented by the red triangle on b and c., and d. Temporal coverage of the $PM_{2.5}$ sampling campaign with white patches denoting no-sampling days.

its height ranges from 1300 masl (meters above sea level) in the valley to 2800 masl at the western mountaintop. By 2018, the population in the AV reached 3.73 million inhabitants, with a dense conurbation. Due to the accelerated urban expansion

90 (Echeverri and Orsini, 2011; Salazar Hernandez et al., 2022), the increasing vehicular fleet (Corrales Espinosa et al., 2016), and the limited air pollutant dispersion, the valley air quality status represented by $PM_{2.5}$, frequently exceed strict local and international air quality 24-h standards (WHO, 2021, 15 $\mu g/m^3$). Hence, the addition of external pollution sources has caused severe air quality episodes in the valley (SIATA, 2021).

The AV has two rainy periods responding to the latitudinal migration of the Intertropical Convergence Zone (ITCZ), with

95 maximum precipitation during April and November and minimum during January and July. In the transition period, February and March are characterized by persistent atmospheric stability and a thinner atmospheric boundary layer enhancing the accumulation of air pollutants (Herrera-Mejía and Hoyos, 2019). During this period of dry conditions, fires are more likely to spread in NSA, which affects air quality in the AV and neighboring regions (Mendez-Espinosa et al., 2019; Henao et al., 2021). These conditions modulate the intra-annual variability of $PM_{2.5}$ and PM_{10}. In this period, the transport and environmental local

100 authority (Área Metropolitana del Valle de Aburrá) implemented special control on mobile sources, limiting daily vehicle use.

2.2 Data sources

2.2.1 PM$_{2.5}$ chemical campaign

A sampling campaign was conducted at an urban background station from April 3, 2019, to October 5, 2022, to characterize chemicals on PM$_{2.5}$ filters. A total of 247 daily noon-to-noon PM$_{2.5}$ samples were analyzed and described. While April 2019 to July 2020 represented an intense sampling campaign with samples every three days, the frequency of the surface site observations became more sporadic after July 23, 2020, due to several factors. This resulted in several large data gaps in the second half of the time series. However, the sampling in this later period was typically between 3 to 14 days. Therefore, while the temporal sampling resolution did decrease with time, we still have periods of intense sampling and measurements across the majority of the period. Thus, we still have retrieved sufficient and suitable quality data for our analysis in this study.

The samples were taken in Belén, Medellín, on the western slope of the valley by the laboratory GYGHAM, close to MED-BEME, a station of the official air quality monitoring network (see Fig. 1c). Although some brick factories exist, the zone's economy is based on service and small business. Both the residential and closer brick factory areas are around 250 m from the station. According to Gómez-Marín et al. (2021), the primary sources of PM$_{2.5}$ in MED-BEME are the ceramic industry (22.2%), emissions from BB (21.9%), diesel (13.6%), gasoline combustion (12.8%), incineration (1.7%), and coal-fired boilers (16.3%).

The campaign considered minerals (Be, Na, Mg, Al, Si, K, Ca, Ti, V, Cr, Mn, Fe, Co, Ni, Cu, Zn, As, Se, Mo, Ag, Cd, Sb, Ba, Hg, Pb), anions (F$^-$, SO$_4^{2-}$, NO$_3^-$, Cl$^-$), cations (K$^+$, Mg^{2+}, Ca^{2+}, Na$^+$), and carbonaceous matter species (OC1, OC2, OC3, OC4, OC5, Pyrogenic Carbon- PyC, EC1, EC2, EC3, EC4, EC5, EC6, OC, EC, C). In particular, cations were measured only in 207 of the 247 sampling days. Fig. 1d shows the temporal distribution of the samples throughout the study period. An exception for minerals is Na, Mg, K, Se, Ca, and Hg, whose measurements were finished in March 2021. The elements were analyzed from an 8"x10" quartz filter in a High Volume PM$_{2.5}$ ambient air sampler (Reference: PM$_{2.5}$HV - Tisch Environmental). An inductively coupled plasma mass spectrometry and thermal/optical transmission (TOT by NIOSH 5040) were used to measure minerals and carbonaceous matter. Ionic chromatography (IC) was used for both anions and cations. Official campaign concentrations of PM$_{2.5}$ were measured by a Low Volume PM$_{2.5}$ ambient air sampler. Further details on the techniques and the support of laboratory protocols are described in Gómez-Marín et al. (2021).

In addition to the carbonaceous matter, species measured included secondary organic carbon (SOC), which is used in this study. The elemental carbon trace methodology (Huntzicker et al., 1986) was used for calculating the SOC. This method assumes that the organic carbon measured comes from the background, primary, and secondary sources and hence follows the relation described by Equations 1 and 2.

$$POC = OC_{back} + EC \times (OC/EC)_{pri} \qquad (1)$$

$$SOC = OC_{Total} - POC \qquad (2)$$

Where POC represents the primary organic carbon, OC_{back} is the background, OC_{total} is the consolidated OC measured in the campaign, and $(OC/EC)_{pri}$ is the primary ration between OC and EC.

135   Equation 1 describes a linear relation of primary carbon matter compositions. The linear model was calculated using the 20th percentile OC and EC concentrations, aligned with Yao et al. (2020); Lin et al. (2009). The process was repeated for each hydrologic trimester (DJF, MAM, JJA, and SON) due to the influence of weather conditions in the region. The resulting slope is interpreted as $(OC/EC)_{pri}$, and the intercept is the OC_{back}. After calculating the $(OC/EC)_{pri}$ and OC_{back}, Equation 1 was used for calculating every sampling day POC using the sampled EC. Then, the SOC was obtained with Equation 2.

140   This study involved creating four different linear regression models (Equation 1) for the two yearly dry (June-August and December-February) and rainy (March-May and September-November) periods. The square of correlation coefficient (R^2) showed high performance of the models with values ≥ 0.95.

2.2.2   PM$_{2.5}$ concentrations

In addition to the campaign data, we used we used daily PM$_{2.5}$ data come from the official air quality monitoring net-
145   work operated by the local early-warning system – SIATA (SIstema de Alerta Temprana de Medellín y el Valle de Aburrá, https://siata.gov.co/). These hourly PM$_{2.5}$ concentrations, from April 2019 to October 2022 in our study, from the MED-BEME station coincided with the site of the chemical sampling campaign (illustrated in Fig. 1b). Daily average concentrations were calculated matching the sampling schedule (noot-to-noon). Only days with at least 75% of the hourly data were processed. Within our study period, we derived valid daily average concentrations for 96.7% of the days investigated. The Pearson corre-
150   lation coefficient between the PM$_{2.5}$ measured by the campaign and the network was 0.84, with a mean absolute percentage error of 21.5%.

2.2.3   CAMS Reanalysis dataset

The European Centre for Medium-Range Weather Forecasts (ECMWF) provides atmospheric composition datasets through the Copernicus Atmospheric Monitoring Service (CAMS; Inness et al., 2019). For this research, we utilized the ECMWF
155   Atmospheric Composition Reanalysis-4 (EAC4) dataset. It is a global atmospheric chemistry model, simulating a range of key tracers of composition, which uses a 4-dimensional variational data assimilation to assimilate satellite retrievals of, e.g., aerosol optical depth (AOD), carbon monoxide (CO), nitrogen dioxide (NO$_2$) and ozone (O$_3$) (Inness et al., 2019).

    CAMS simulates different aerosols, which complete the total AOD at 550 nm and different gases. To identify considerable loads from biomass burning (BB), dust, and volcanic aerosols, respectively, this study considers two AOD fractions: dust
160   AOD (Du-AOD) and organic matter (OM-AOD), in addition to the total column sulfur dioxide (TCSO$_2$). The products were downloaded daily at the original 3-hourly resolution and then resampled for local noon-to-noon periods aligned with the sampling campaign schedule. Only pixel information over the sampling site was used.

2.2.4 Meteorological data

Meteorological data come from the ECMWF Reanalysis v5 (ERA5; Hersbach et al., 2020). Fields of zonal and meridional
165 winds, temperature, and moisture were obtained at temporal and spatial resolutions of 3 hours and 0.25° (approximately 27
km), respectively. ERA5 data were up-sampled to a daily frequency to guarantee consistency with the chemical sampling. Due
to poor performance in representing precipitation in the region by reanalysis (Posada-Marín et al., 2019), satellite-based fields
were retrieved from the Global Precipitation Measurement (GPM) daily final precipitation product (Huffman et al., 2019) with
a spatial resolution of 0.1°.

170 Further, a back trajectories dataset was built from the chemical sampling point. 8-day trajectories starting at heights of 800
hPa, 750 hPa, and 700 hPa were run every 3 hours with a time step of 3 hours. The model only uses wind data from the
products 4h-daily pressure levels U-wind, V-wind, and omega (with a spatial resolution of approximately 2.5^{o}) from NCEP-
NCAR Reanalysis 1 (https://psl.noaa.gov). The model follows Equation 3. for estimating every back position.

$$X(t - \Delta t) = X(t) - V(X,t)\Delta t \qquad (3)$$

175 Where X is the location with vertical and horizontal coordinators, V is the wind vector, and t is the time.

2.3 Identification and tracking of aerosol events

2.3.1 Identification of LRT events

Despite the selected CAMS products covering the whole atmospheric columns and not only the surface, CAMS has a high
predictive capability for PM$_{2.5}$ in the AV (Pérez-Carrasquilla et al., 2023). Furthermore, its products relatively reasonably
180 reproduce PM$_{2.5}$ tendencies and extreme events in the territory (Casallas et al., 2022). Therefore, the magnitude of CAMS
products OM-AOD, Du-AOD, and TCSO$_2$ in the AV were utilized to identify possible BB-LRT, Dust-LRT, and Volcanic-LRT
events, respectively.

To help identify PM$_{2.5}$ days that were subject to long-range transport, the time series of the CAMS data sets were stan-
dardized. Here, for each day, the time-series average (mean) was subtracted from the daily value and then normalized by the
185 time-series standard deviation (i.e., 1 σ). This then allowed for the identification of LRT events using a range of subjective
thresholds and the quantification of the corresponding PM$_{2.5}$ concentrations and composition. The thresholds investigated
ranged from 0.8 to 2.0 σ, but in this study, we present the results for thresholds of 0.8, 1.5, and 2.0 σ. To help accurately
identify periods of LRT events and remove short-term sporadic events, a 7-day running window was used. Here, if less than
four days with values greater than the specified threshold were detected, then they were classed as outliers and removed (i.e.,
190 we are focussing on LRT events, which we define as lasting more than half a week). Observe that continuous days marked as
peaks are possible for longer-lasting events. Finally, for each peak event (DtE), the surrounding days, relative to the peak event
centered in the 7-day window (i.e., DtE$_0$), were labeled. For instance, the LRT events ranged from three days before (DtE$_{-3}$)
to three days after (DtE$_3$) the peak event. The days outside of three-day windows around a DtE$_0$ are generally identified as

no-event days, and no significant/lasting event affectation is supposed. Although the process described above was run for every
event and threshold, further assessments are based on 0.8 σ for BB-LRT and 1.5 σ for Dust-LRT and Volcanic-LRT, as is
described in Section 3.1.

2.3.2   Regional meteorological analysis

A regional analysis of meteorological fields was performed during pollution LRT events to identify conditions that favor aerosol
transport from the sources of interest. We computed anomalies for each pixel of the meteorological fields by subtracting the
average of the corresponding month from the original values in the study period. Subsequently, composites during days with
events (DtE$_{-3}$ to DtE$_3$) were performed with meteorological fields and anomalies for each source. This approach helps reveal
particular conditions during days with aerosol LRT events. The results are also supported by analyzing air masses arriving at
the AV using back-trajectories during the events. The number of times trajectories pass through a pixel was counted to estimate
a percentage indicating the influence area.

2.3.3   Influence on local PM$_{2.5}$ concentrations

The local measurements of PM$_{2.5}$ were used to assess the influence of CAMS-based identified events on air quality in the AV.
The daily PM$_{2.5}$ datasets were labeled with the days to the closest event peak (DtE) to compare concentrations before and after
the events. The days before the event constitute from 15 to 4 days before the event peak (DtE$_{-15}$ to DtE$_{-4}$), while the days
after the event peak consisted of 4 to 15 days after the event peak (DtE$_4$ to DtE$_{15}$). These ranges were determined to have
enough data from the chemical campaign on similar weather conditions for comparison between the days affected by the LRT
of aerosols and the days before and after. We used the Mann-Whitney U test to compare these periods. The null hypothesis is
denied with the confidence of 90% (p-value $\leq$ 0.1) and 95% (p-value $\leq$ 0.05).

The COVID-19 lockdown period (April 1st to June 1st, 2020) was filtered from our record to avoid perturbation out of
standard emission patterns in the region.

2.3.4   PMF and PM$_{2.5}$ chemical composition

The Positive Matrix Factorization (PMF) is a receptor model developed by the EPA (Environmental Protection Agency) to
analyze water and air samples. The model expresses observations of PM$_{2.5}$ as a sum of the contributions from a number of
source profiles (non-time dependent). In this case, we are using the PMF model and our campaign measurement data of PM$_{2.5}$
chemical composition and PM$_{2.5}$ concentrations to identify the dominant sources (e.g., coal combustion, vehicular emissions,
secondary pollution) during different LRT classed events (i.e., BB, dust or volcanic LRT events). For the AV, 5 to 7 factors
(i.e., sources) have been suggested (see Gómez-Marín et al. (2021)).

The PMF is mathematically expressed as (Paatero and Tapper, 1994):

$$X_{ij} = \sum_{k=1}^{N} g_{ik} f_{kj} + e_{ij} \tag{4}$$

8

The objective of PMF is to determine the values of g_{ik}, f_{kj}, and N (i.e. the number of factors) that best reproduce X_{ij}.

Here, X represents the measurement data for sample i (daily temporal resolution) and chemical component j. An inversion approach is used for this matrix problem, exploiting an iterative scheme to converge on the solutions for g_{ik} and f_{kj}. In the factorization problem, f_{kj} contains the concentration of each chemical component (j) in the unit profile for the factor k (i.e. $PM_{2.5}$ source). The matrix $g_{i,k}$, the contribution factor, defines how much of the profile is counted in the total concentration in day i. $e_{i,j}$ contains the residual for each compound/sampling day. Outputs from the PMF include statistical metrics that help to evaluate the model performance, such as the correlation coefficient (R^2), the recuperated mass (% RM), and the objective function value (Q). The PMF adjusts g_{ik} and f_{kj} to minimize the function Q in Equation 5 (Paatero, 1997).

$$Q = \sum_{i=1}^{n} \sum_{j=1}^{m} \left[\frac{X_{ij} - \sum_{k=1}^{N} g_{ik} f_{kj}}{\mu_{ij}} \right]^2 \tag{5}$$

Where μ_{ij} contains the uncertainty compound/sampling day.

The model uses two input uncertainties. The first is the species uncertainty (μ_{ij}), which does not change in the process and is according to the method unique for every species sample. In this study, μ_{ij} considers the measurement and analytical errors, comprising uncertainties of the volume of air processed, filter area, and species mass, in addition to the uncertainty of the detection limit of the measurer method. The last one represents the analytical uncertainty and was calculated following US-EPA (2014) by using the methods detection limit suggested by Eugene Kim and Qin (2005). However, for $PM_{2.5}$, we followed the approach of Eugene Kim and Edgerton (2003) who set μ_{ij} (where j represents $PM_{2.5}$ for day i) greater than the daily $PM_{2.5}$ concentration (i.e., three times the concentration in this study). The second uncertainty in μ_{ij} is recognized as the "Extra modeling uncertainty". It is added to the model as a percentage to cover other inherent errors, such as variations of source profiles and chemical transformations in the atmosphere. A range from 10% to 16% was tested for the models of every kind of LRT event; this aligns with other studies (Callén et al., 2009; Shin et al., 2022; Salim et al., 2019).

During the modeling process, species can be classified as "strong" "weak," or "poor" based on individual statistics. The "weak" category triples the uncertainty μ_{ij}, and the "bad" excludes the species from the model. Two statistics are key for categorizing the species. First, the signal-to-noise ratio (S/N) represents overall uncertainty per concentration. S/N<0.5 is generally classified as "bad" because the uncertainty surpasses two times the concentrations (US-EPA, 2014). Second, the regression diagnostic where R^2 informs about the linear relation of every species' observed and modeled concentration.

The model convergence evaluation statistics considers this classification with the $Q/Q_{expected}$ ratio. $Q_{expected}$ is the theoretical value of Q (Equation 5), expressed as Equation 6.

$$Q_{expected} = (n \times m_s) - ((N \times n) + (m_s \times N)) \tag{6}$$

where n is the number of sampling days and m_s is the number of "strong" species use for modeling (US-EPA, 2014).

Due to missing data, all species except cations are included in the model. Only total OC and EC from carbonaceous matter are included for Duts-LRT and Volcanic-LRT events since comprising all carbon species could particularly weigh those and

Table 1. Statistics of OM-AOD, Du-AOD, and TCSO$_2$ representing BB-LRT, Dust-LRT, and Volcanic-LRT

Threshold	Events stats.	OM-AOD	Du-AOD	TCSO$_2$
0.8 σ	Samples	31	31	59
1.5 σ	Samples	18	19	32
2.0 σ	Samples	10	4	21
0.8 σ	Limit	0.22	0.01	$0.70 mg/m^2$
1.5 σ	Limit	0.28	0.02	$0.87 mg/m^2$
2.0 σ	Limit	0.32	0.02	$0.99 mg/m^2$
0.8 σ	Average	0.25	0.02	$0.78 mg/m^2$
1.5 σ	Average	0.29	0.02	$0.88 mg/m^2$
2.0 σ	Average	0.32	0.03	$0.97 mg/m^2$

"Samples" represent the number of sampling days available for the PMF characterization.
Each threshold limit defines the calculated absolute magnitude. Note, AOD is a
dimensionless quantity.

overshadow trace elements for the sources. For those LRT events, the potential run period is reduced until April 2021 since the tracer minerals Na, K, and Mg were not measured afterward.

The factor interpretation of this study was primarily supported by the source characterization made by Gómez-Marín et al. (2021) for the studied station.

A final element comparison is made between the days of events with a positive relative contribution ($g_{i,k}$>0) and the days categorized as before (DtE$_{-15}$ to DtE$_{-4}$) and after events (DtE$_4$ to DtE$_{15}$).

3 Results

This section is divided into four subsections. The first subsection shows possible aerosol events from BB-LRT, Dust-LRT, and Volcanic-LRT. The second is focused on the temporal and regional characterization of the events, including a description of meteorological patterns and possible sources of aerosols. Finally, the third and fourth subsections locally assess the identified events using ground-level PM$_{2.5}$ concentration and chemical compositions, respectively.

3.1 Identification of events

The products OM-AOD, Du-AOD, and TCSO$_2$ from the CAMS reanalysis were used to identify aerosol from BB-LRT, Dust-LRT, and Volcanic-LRT, respectively. Tab. 1 shows different statistics about the identification for each kind of event using the threshold of 0.8 σ, 1.5 σ, and 2.0 σ. The intensest events reached maximum magnitudes of 0.66 for OM-AOD (March 30, 2020), 0.11 for Du-AOD (June 24, 2020), and 1.96 mg/m^2 for TCSO$_2$ (September 10, 2022). These specific days exceeded the average values for identified events more than twice for OM-AOD and TCSO$_2$ and more than five times for Du-AOD.
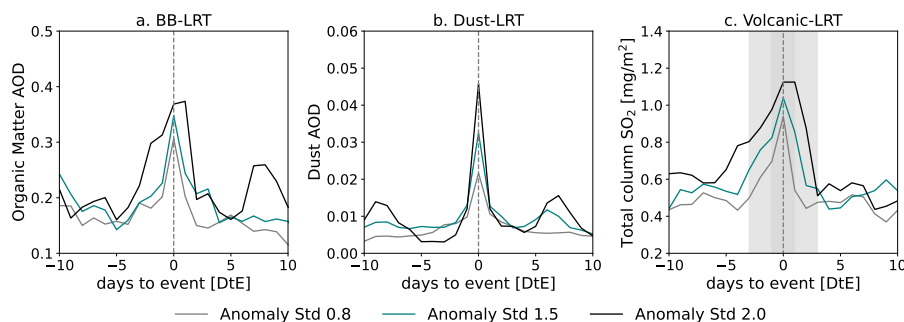
Figure 2. Average magnitudes of OM-AOD (a.), Du-AOD (b.), and TCSO$_2$ (c.) concentration around the events. Different colors represent different anomalies. The shadowed region delimits the event. Du-AOD is on a scale that is ten times lower than OM-AOD.

Notably, OM-AOD reached 77% of the total AOD in the intensest event. Regarding the variability, all identified events showed high variability with a standard deviation around 42%, 90%, and 35% of the average for OM-AOD, Du-AOD, and TCSO$_2$, respectively.

Fig. 2 shows the average behavior of each variable centered around the event peak for the threshold of 0.8 σ, 1.5 σ, and 2.0 σ. The events exhibit a clear peak centered on DtE$_0$ for most of the considered threshold. However, events identified with 2.0 σ exhibit noisy behavior around the peak for BB-LT and volcanic-LRT. In particular, OM-AOD exhibits a second peak after the event peak. This could be caused by either the smaller sampling size or high aerosol loads that do not meet the duration criteria for the threshold. Besides, the strictest thresholds (2.0 σ) result in a considerable reduction of studied events (see Tab. 1), which is critical for the assessment of $PM_{2.5}$ chemical composition.

Based on the study's objectives, only one identification threshold was selected for each event, allowing the investigation of more accurate identification indexes. Based on the results and literature review about the expected frequency of each type of event for the city (Mendez-Espinosa et al., 2019; SIATA, 2021), we selected events that exceed 0.8 σ for BB-LRT and 1.5 σ for Dust-LRT and Volcanic-LRT. Anomalies over 2.0 σ significantly limited the number of days for the analysis, whereas 0.8 σ probably oversamples volcanic and dust aerosol load events, whose affectation is recorded as infrequent. Moreover, the selection ensures yearly representativity for each event (see supplementary Figure S2). BB-LRT, Dust-LRT, and Volcanic-LRT were represented during the complete study period, at least for three years each. Notably, in 2020, these events covered 19.4%, 6.6%, and 12.0% of the days, respectively. With this selection, the sampling campaign can represent BB-LRT, Dust-LRT, and Volcanic-LRT events in the PMF with 31, 19, and 32 samples.

3.2 Regional analysis of events

Regional analysis was conducted to establish the meteorological conditions that may favor pollution LRT events and identify potential aerosol sources. The average spatial distribution of the identified AOD-OM, Du-AOD, and the TCSO$_2$ during the aerosol LRT events is shown in Fig. 3, with the integrated back trajectories of air masses arriving at the AV. OM-AOD values
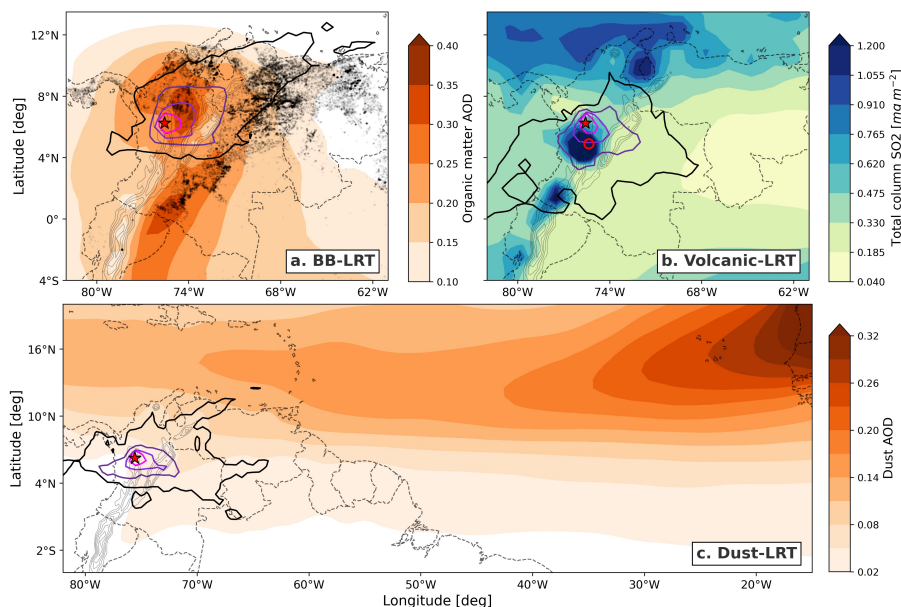
Figure 3. Mean spatial distribution of OM-AOD (a.), TCSO$_2$ (b.), and Du-AOD (c.) for days with each type of LRT event. Pink-to-black contours enclose the regions from which 20, 10, 5, and 1% of air masses arrive at the AV according to the back-trajectories. Gray dots in a. show MODIS-retrieved hotspots associated with fires with a 70% of confidence. The red star marks the location of the AV, while the red circle in the upper right panel is the location of the Nevado del Ruíz Volcano. The black contours show the terrain elevation from 1500 to 5000 masl.

above 0.2 occur over most of Colombia during BB aerosol events (Fig. 3 a), consistent with a high number of fire hotspots
295 in northern South America (Venezuela and Colombia). In particular, the back trajectories during these days suggest that a large part of the air masses arriving at the AV (10 to 20 %) come from the northeast, where OM-AOD exhibits its maximums (exceeding magnitudes of 0.35).

Volcanic-LRT (Fig. 3 b) shows high SO$_2$ values (over 1.2 $mg\,m^{-2}$) in the atmospheric column above the Nevado del Ruiz volcano (red hollow circle). Additionally, another two spots are evident: the first one, toward southwestern Colombia, could be
300 related to another degassing volcano called the Galeras, whereas the other one is on Maracaibo Lake, with relatively high values possibly associated with oil extraction (see Fioletov et al. (2016)). According to the back-trajectories, during Volcanic-LRT events, around 10% of the air masses arriving in the AV come from the southeast, where the Nevado del Ruiz hotspot exists. A smaller fraction of air masses (1%) arrive from the hotspot in the country's southwest. Similarly, a clear dust propagation pattern is evident from the Sahara desert towards the Caribbean and, to a lesser extent, NSA (see Fig. 3 c). While air masses for
305 BB-LRT and Volcanic-LRT have different directions, most air masses that reach the AV during Dust-LRT events come from the east, showing consistency in the analysis.

Despite the short study period, the identified events suggest a marked annual cycle (Fig. 4). During March, 50.0% of studied days represent the BB-LRT. April and February also showed high proportions of this event, with 43.3% and 24.8%. Concerning

the dust events, two maximums are observed, April and July, with a proportion of 23.3% and 23.4%. The distribution for

310   volcanic-LRT ranges from June to September, with a clear peak in August with a frequency of 49.2%. Additionally, as shown

in Fig. 4, external events overlap in some cases. The higher intersections observed were for BB-LRT and Dust-LRT in April and

for BB-LRT and volcanic-LRT in September. Here, where days were defined as both, e.g., BB-LRT and Dust-LRT, they were

added to the joint classification (i.e., BB-LRT & Dust-LRT) and were not included in the respective singular classifications.

Overall, the annual cycle of these frequencies and the local $PM_{2.5}$ concentration show the event's possible influence on $PM_{2.5}$

315   is non-linear.
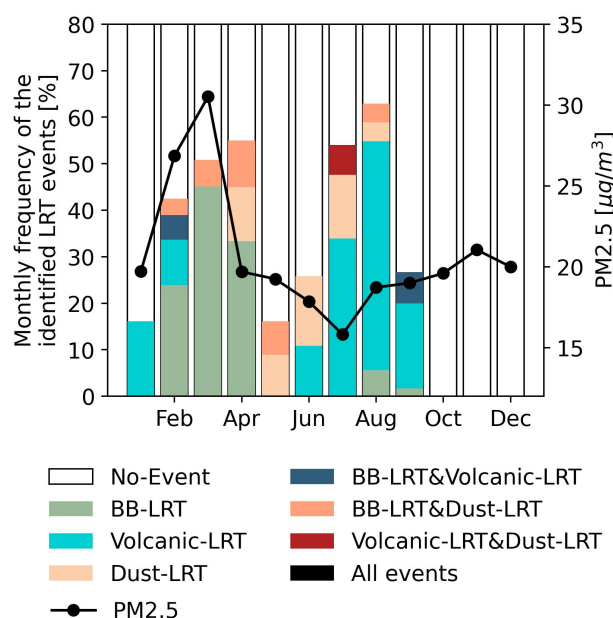
Figure 4. Monthly frequency of CAMS-based identified BB-LRT (green bars), Dust-LRT (wheat color bars), and volcanic-LRT (blue bars).
Overlapped events are depicted in dark blue, orange, red, and black bars, while the white fractions represent the period of no identified events.

Although LRT events exhibited a marked season, some non-event days in the different months occur (see Fig. 4), suggesting

that intraseasonal variations are also relevant. To elucidate specific meteorological patterns during events days, Figs. 5 and 6

present composites of meteorological variables for the low (800 to 700 hPa) and mid (600 to 400 hPa) troposphere for the

different kinds of events. The Andes mountain range generally causes a large spatial variability in the low-level wind field. The

320   winds blowing from the east of the Andes cross the mountain range through two zones with relatively low altitudes (hereafter

mountain passes), which are demarcated with white boxes (see Figs. 5 a, b, c).

Anomalous dry winds of around 1 m/s originate from the north during BB-LRT events (Fig. 5 d), connecting the AV with

the high OM-AOD region. Additionally, winds blowing from Venezuela, where multiple BB hotspots were identified, reach

northern Colombia through the mountain pass located north of the Andes, at the border between Colombia and Venezuela (see

325   Fig. 5 a). Low-level winds during LRT events are in agreement with the back trajectories of Fig. 3 a. A reduction of 2 to 3 m/s
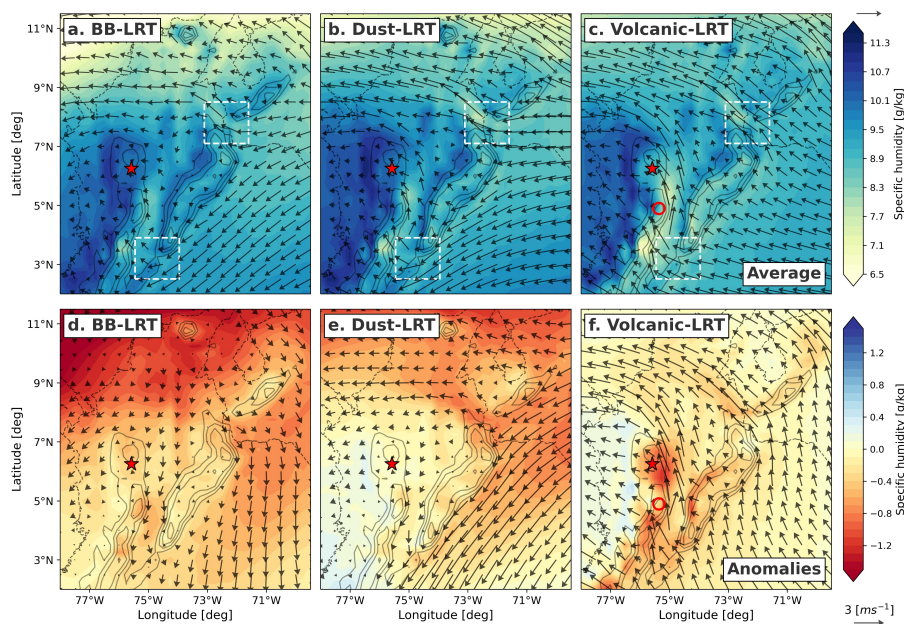
Figure 5. Meteorological composites for low-level (800 to 700 hPa) winds and specific humidity during days with (a.) BB-LRT, (b.) Dust-LRT, and (c.) volcanic-LRT events. d, e, f: as upper panels but for anomalies. A red star marks the Aburrá Valley, and the red circle in the upper right panel is the Nevado del Ruíz volcano. The white rectangles are two mountain passes in the Colombian Andes. The black contours show the terrain elevation from 1500 to 5000 masl.

in the intensity of mid-level winds (between 5°N and 8°N; see Figure 6 a, d) was also observed along with less rainy conditions in northern Colombia.

For Dust-LRT events, low-level winds flow across the two mountain passes in the Andes (Fig. 5 b) with increased easterly winds north of Colombia and northeasterly winds east of the Andes (Fig. 5 e), representing a dry flow from the Atlantic Ocean
330   where Du-AOD is higher. Figs. 6 b and e, show that mid-level winds have notable eastward direction with anomalous winds coming from the Caribbean and less rainfall in NSA.

Finally, days with volcanic-LRT events are characterized by southeasterly winds blowing toward the AV (see Fig. 5 c) from the Nevado del Ruíz volcano region. These winds may be favored by anomalous southeasterly winds of more than 3 m/s crossing the southern mountain pass, as shown in Fig. 5 f, along with drier air reaching the AV. Less rainy conditions are also
335   present in the Colombian Andes (Fig. 6 f), particularly between the AV and the Nevado del Ruíz volcano.

Noteworthy, the three types of events are accompanied by less rainy and drier atmospheric conditions in northern Colombia, Venezuela, and the Andes, respectively, with rainfall anomalies greater than -4 mm/d and specific humidity anomalies up to -1 gkg^{-1}. These results allow us to highlight the importance of precipitation to enhance or even trigger the aerosol LRT events to the AV.
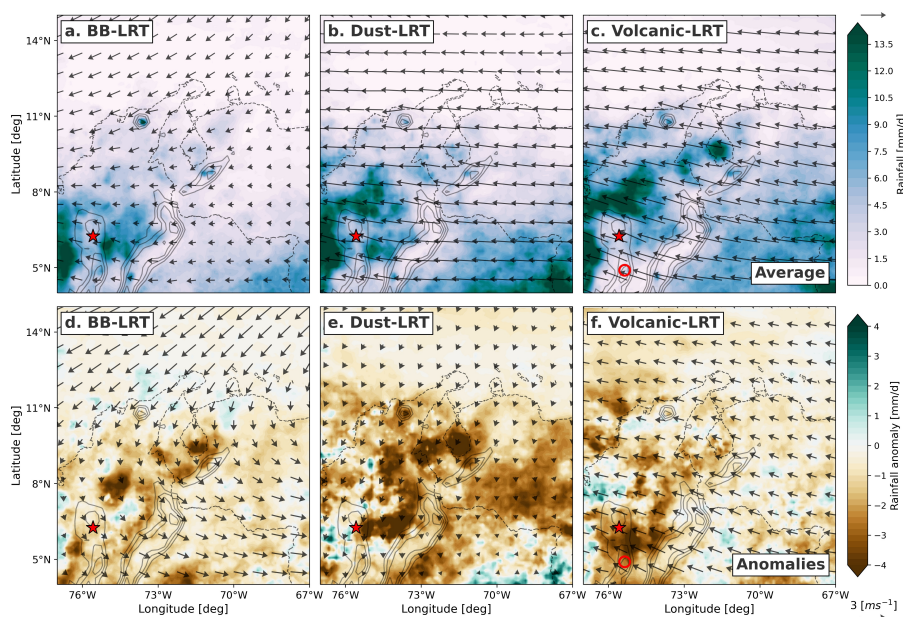
14

Figure 6. Meteorological composites for mid-level winds (600 to 400 hPa) and rainfall during days with (a) BB-LRT, (b) Dust-LRT, and (c) Volcanic-LRT events. d, e, f: as upper panels but for anomalies. The red star marks the Aburrá Valley, and the red circle in the upper right panel is the Nevado del Ruíz volcano. The black contours show the terrain elevation from 1500 to 5000 masl.

3.3 PM$_{2.5}$ concentrations change

After identifying possible LRT events and the meteorological conditions favoring them, a local analysis was performed to connect and validate the different events' influence on AV's local air quality. The daily concentration of PM$_{2.5}$ reasonably responds to the BB-LRT identified by OM-AOD. Fig. 7 compares the PM$_{2.5}$ concentrations before (DtE$_{-15}$ to DtE$_{-4}$), during (DtE$_{-3}$ to DtE$_3$) and after (DtE$_4$ to DtE$_{15}$) each event. BB-LRT had the highest PM$_{2.5}$ increments, especially at DtE$_0$. 86.7% of values during the peak day exceed the average PM$_{2.5}$ for the study period (20.25 $\mu g/m^3$). Besides, over half of PM$_{2.5}$ concentration during DtE$_0$ exceeds twice the WHO (2021) guidelines for daily concentrations (15 $\mu g/m^3$). On DtE$_0$, the PM$_{2.5}$ average concentrations (31.48 $\mu g/m^3$) were significantly higher than the surrounding days (p-value $\leq$ 0.05), according to the Mann-Whitney test. Similarly, the event days before the peak (DtE$_{-3}$ to DtE$_{-1}$) had significantly higher concentration compared to days before and after the identified BB-LRT events (p-value $\leq$ 0.05). In contrast, concentrations following the event peak are similar to the average magnitude, indicating a sudden decrease.

As for BB-LRT, the peak of the events for Dust-LRT showed higher concentrations than days before the event (p-value $\leq$ 0.1). On the other hand, the increase of PM$_{2.5}$ due to Volcanic-LRT was consistent throughout the event, not just during the peak. After the events, the PM$_{2.5}$ concentration for Dust-LRT remains at similar levels. However, outliers are observed after the events, particularly in March 2020, a period strongly affected by BB-LRT. On the other hand, the concentration of PM$_{2.5}$ right after Volcanic-LRT significantly decreases. Although, forward days (Dte$_8$ to Dte$_{15}$) present an average magnitude similar
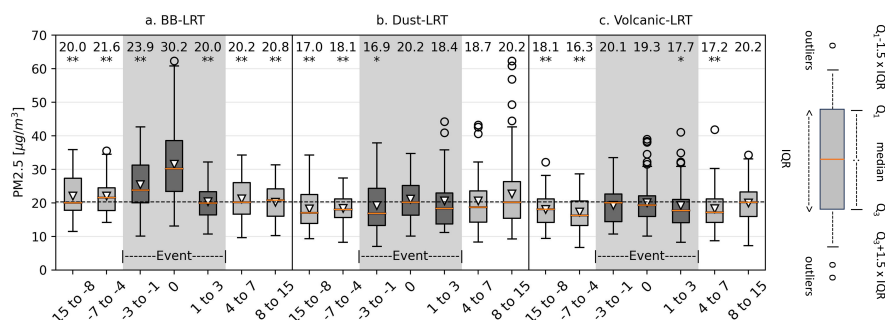
Figure 7. PM$_{2.5}$ concentrations before, during and after (a.) BB, (b.) dust and (c.) volcanic aerosols events. The chart's top presents the median concentration of each dataset, along with the significance level compared with the peak of the data, ≤ 0.1 (*) or ≤ 0.05 (**). The shadowed darker boxes represent the events. The down triangles represent the average concentration for each day range, and the grey dashed line represents the total study period average. The boxes are limited by the first and third quartile, Q$_1$ and Q$_2$

to during the events. Overall, it is clear that the BB-LRT event has a higher impact on PM$_{2.5}$ concentration to the AV than Dust-LRT and Volcanic-LRT.

3.4 PMF and chemical composition change

The PMF models of the BB-LRT and Volcanic-LRT presented low residual responses to no outlier values. For the Dust-LRT, three days were marked as outliers and removed. In general, the three final selected PMF models show a good performance meeting acceptance criteria with a reconstructed mass (RM) in the range of 80 to 120 and an R^2 coefficient greater than 0.8 (US-EPA, 2014). The Q/Q$_{expected}$ for the selected models were close to 1, a determinant parameter for the number of factors and the component categorization. A summary of the models' statistics is given in Table 2.

The results from the PMF for BB-LRT ascribed concentration to six emissions sources (or factors): BB (37.6%), coal boiler (20.1%), ceramic industry (16.7%), gasoline (12.8%). Diesel (11.4%) and Incineration (1.4%). The factor of contribution for BB-LRT in the sampling days varies from 0.0 to 4.5 (maximum identified on 25 March 2020), which means that not all identified event days are backed by the PMF (The factor of contribution for the models ran are in Supplementary Figure S4). Of the 31 samples identified, 27 days (equivalent to 87.0%) have positive contributions from BB abscrited. The PMF profile of the BB factor, represented in Fig. 8a, is identified by the dominant contribution ($\geq 30\%$) of OC species, PyC and some anions. The identified contribution of this factor in OC, but especially in OC1 (50.9%) and OC2 (46.1%), agrees with observations made by Chow et al. (2004) for vegetation burning. Similarly, the high contribution of CyP (43.0%) back the profile since BB produces $\sim$50% of global CyP emissions (Santín et al., 2016). Regarding anions, the contribution to F$^-$ (42.1%) head contribution and support the identification and hypothesis of LRT as a trace element with high lifetime (Jayarathne et al., 2014). The contribution to SO$_4^{2-}$ (37.7%) and NO^{3-} (22.0%) evidence secondary pollutants formation from the BB emissions during daytime and nighttime, respectively (Rastogi et al., 2014). Moreover, the influence over Cl$^-$ concentration (35.7%) may

Table 2. Statistics performance of PMF for models during days affected by BB-LRT, Dust-LRT, and Volcanic-LRT

Properties	BB-LRT	Dust-LRT	Volcanic-LRT
Samples	31	16	32
N. factors	6	6	6
Non-weak species	32	27	27
Bad species	OC5,EC6	Be	—
$Q/Q_{expected}$	0.99	1.00	0.93
Add. uncertainty[%]	16	11	12
Results $PM_{2.5}$			
$PM_{2.5}[\mu g/m^3]$	11.14	6.77	6.46
$PM_{2.5}[\%]$	37.61	33.93	30.85
$PM_{2.5}$ error $[\mu g/m^3]$	2.50	1.84	2.60
R^2	0.92	0.90	0.77
RM [%]	99.31	98.24	97.50

evidence semiarid vegetation burning (Andreae et al., 1998). Other species as K (16.2%) traces BB emissions (Yu et al., 2018; Rastogi et al., 2014).

For the Dust-LRT event days, the model identified the dust contribution (33.9%) and others from BB (27.8%), vehicular (12.4%), resuspended material (6.5%), incineration (7.7%), and ceramic (11.7%). Due to only total OC and EC being con-
380 sidered, splitting the vehicular emissions between diesel and gasoline is difficult. The contribution factor for dust varies from 0.0 to 4.1 (maximum identified on 27 February 2020). For this event, 81.2% (13/16 samples) of the identified days exhibited a positive contribution. The dust profile identification is supported by a high contribution (>31.0%) of Al, Ca, Fe, and Si ($\geq$ 0.1 $\mu g/m^3$), as Fig. 8b illustrates. Similarly, Malaguti et al. (2015) highlights Fe, Al, Ca, Ti, and Mg in the fine Sahara's dust aerosols. Ca and Ti are specially weighted for LRT from the Sahara desert since the other elements are more generic
385 crustal aerosol tracers (Martinez-Verduzco et al., 2023; Nicolás et al., 2008). The dust contributes to 52.6% and 37.0% of Ca and Ti concentration, respectively. The profile also diverges from the general crustal material in the contribution of secondary inorganic aerosol as SO_4^{2-} probably from $(NH_4)_2SO_4$ (Varrica et al., 2019; Malaguti et al., 2015), with 33.9% of average concentration in the samples. Likewise, a particular mix between dust minerals and OC (29.7%) might also be a characteristic to identify the dust profile (Aymoz et al., 2004; Malaguti et al., 2015).
390 For the days of Volcanic-LRT events, the model identified 30.8% of volcanic aerosols contribution. Other sources were BB (29.1%), vehicular emissions (15.7%), resuspended dust and ceramic industry (11.0%), secondary aerosol formation (9.1%), and incineration (4.3%). The volcanic factor presented contributions varying from 0.0 to 3.9 (maximum identified on 6 February 2020). According to the model, the volcanic factor influences only 78.1% (25/32 samples) of identified days. As expected Satsumabayashi et al. (2004), the volcanoes profile in Fig. 8c, shows a high contribution of SO_4^{2-} (36.9%). The contribution
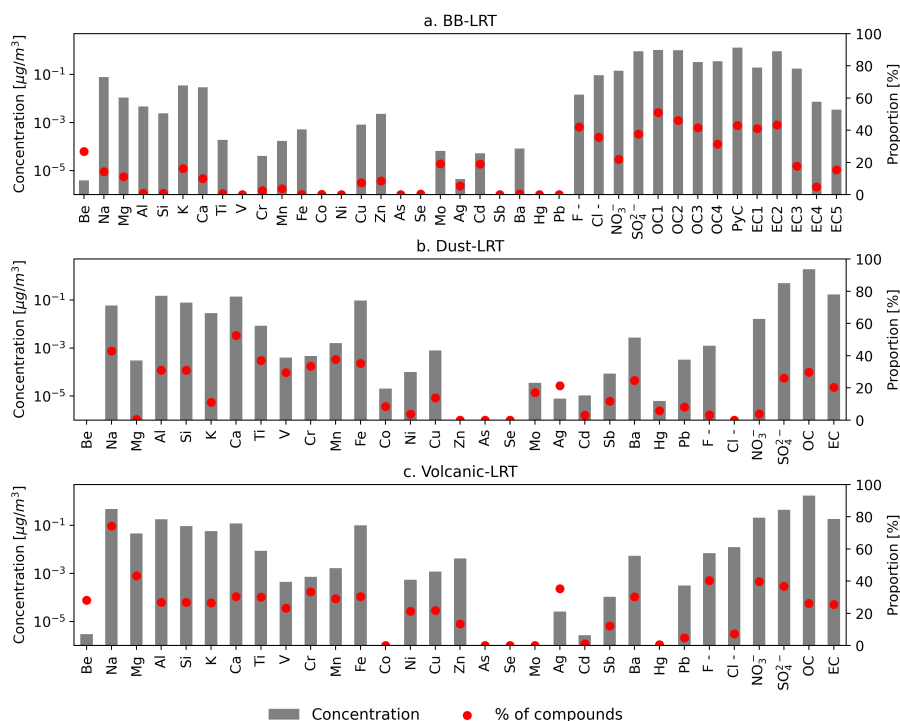
Figure 8. PMF output profiles for (a.) BB-LRT, (b.) Dust-LRT, and (c.) volcanic-LRT events. The bars represent the average concentration of the compounds, while the red points denote the compound's average percentage contribution to the whole element concentrations. Refer to Supplementary Figure S3 to see the contribution of all factors.

395 but not the concentration of SO_4^{2-} was surpassed by F^- and NO^{3-}. F^- from volcanic emissions frequently concentrated onto the ash surface as $CaF2$, $AlF3$ or Na_2SiF_6 (Bia et al., 2020; Delmelle et al., 2021); while may relate with the oxidized trace species HNO_3 (Martin et al., 2012). Minerals with relatively large concentrations in the identified profile include Na, Al, Ca, Fe, Si, K, and Mg in descendent order presented concentration >0.04 $\mu g/m^3$ (contribution of >26.5%). The finding of Trejos et al. (2021) and Vanegas et al. (2021) supported the volcanic profile, with Si, Al, Fe, Ca, K, Mg, and Na as the

400 main minerals for the Nevado del Ruiz Volcano ashes. Although the composition might vary between volcanoes, the results for Sangay volcanic ashes in the region also back up the profile with similar main elements (Moran-Zuloaga et al., 2023). From these, Fe, Al, and Na are the most representative for the ashes diameter < 2.5 μm (Mason et al., 2021); while Ca, Na, Si, and K might be particularly persistent after LRT (Ruggieri et al., 2012).

The total daily composition of $PM_{2.5}$ is also evidence of the impact of the LRT event. Fig. 9 shows the average daily

405 concentration of the campaign-measured data for each kind of event and when no event is identified. This only considers days with a positive contribution factor from PMF results. Although the non-event average concentration is presented, the statistical comparison is made with the days before and after events to maintain similar meteorological conditions (i.e. the combined time-series of before (DtE_{-15} to DtE_{-4}) and after event (DtE_{+4} to DtE_{+15}) is statistically compared to the event time-series (DtE_{-3}
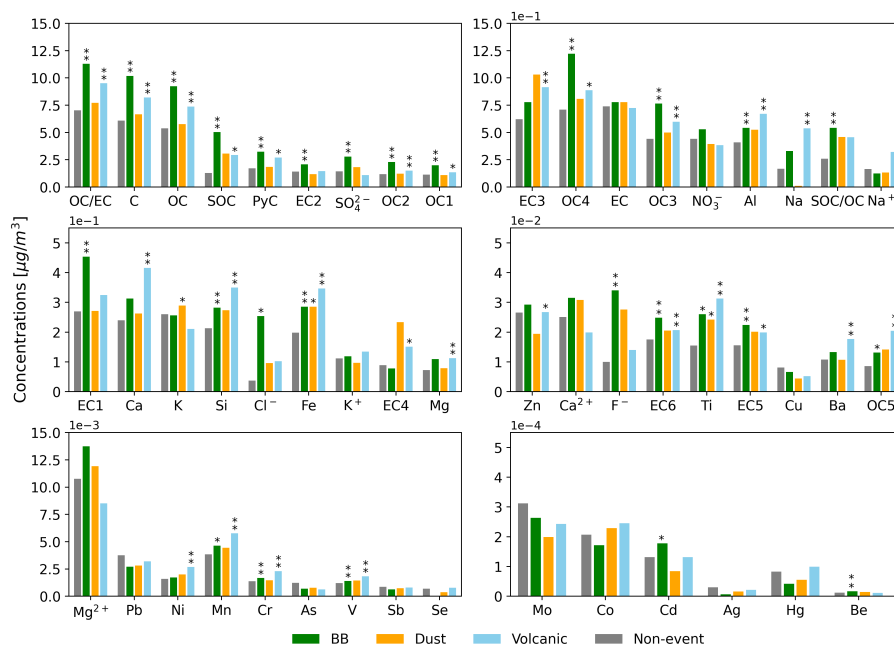
Figure 9. Campaign average concentration for non-event and positive-contribution days for BB-LRT, Dust-LRT, and Volcanic-LRT. The bars represent the concentration of the compounds along with the significance level compared with the days before and after the events, ≤ 0.1 (*) or ≤ 0.05 (**). The y-axes change for every figure to better identify concentrations. Supplementary Table S1 presents these values and the mean concentrations of the compounds for days around (i.e., before and after) each event.

to DtE_{+3}) using the Mann Whitney test. Unlike the PMF model, this comparison contains cations and all carbon matter species characterized for every event and widely used ratios such as OC/EC and SOC/OC. The major elements generally have a more significant increment in LRT events. Some elements supported the model's fingerprint, e.g., OC, OC1, OC2, SO_2^4 for BB; Fe, Al, and Ti for dust; and Si, Al, Fe, Ca, Mg, and Na for volcanic aerosols. The OC was significantly higher for BB, presenting a median OC/EC ratio of 11.3 that surpasses common urban combustion ratios like from fossil fuel ($\sim$4), combustion, and Diesel exhausted (<1) (Pani et al., 2019). Although OC/EC is more commonly used to identify sources of urban combustion and BB, some studies have shown its potential for determining the influence of volcanic activity (Pongpiachan et al., 2019). This is supported by evidence of carbon enrichment resulting from volcanic influence (Martinsson et al., 2009), which is also observed in this study, with consistently high concentrations in all OC species and almost all EC species (EC3, EC4, EC5, EC6). For volcanic aerosols, OC/EC had a median of 9.5. Likewise, the formation of SOC significantly increased for both events, with magnitudes of 5.0 and 2.9 for BB and volcanic aerosols, respectively. Heavy metals Cr (2.30 ngm^{-3}), Ni (2.67 ngm^{-3}), and Mn (5.76 ngm^{-3}) concentrations notably increased in event days for volcanic aerosols. Only the maximum concentration for Ni (25.05 ngm^{-3}) exceeds the concentration limit suggested for the annual average of the compound (20

19

ngm^{-3}) by European Commision (2019). Increments for Mn (4.64 ngm^{-3}) and Cr (1.67 ngm^{-3}), in addition to Cd (0.18 ngm^{-3}), were observed for BB. The (European Commision, 2019) set an annual limit of 5 ngm^{-3} for the Cd average.

425   The elevated concentrations of ions in the days of events also support the profiles selected and align with the literature. For the BB, in addition to the ions discussed, the cations K^+ are representative ions (Rastogi et al., 2014; Moreno et al., 2023) that present significant increments. Regarding the volcanic aerosol compositions, the observed increment on Na^+ and K^+ also align with previous reports (Moreno et al., 2023; Mather et al., 2003; Roberts et al., 2018). On the other hand, although the PMF's fingerprint presented a high contribution of $SO2^{4-}$ and F^-, this was not enough for a significant rise in daily concentrations (Mather et al., 2003).

430 ## 4   Discussion

Our analysis focused on events with high aerosol load and frequency, supported by a relatively long $PM_{2.5}$ chemical composition record. This approach avoided restricting the study to short periods (i.e., sporadic singular large-scale events) and made it possible to quantify longer-term and more frequent events (i.e., the long-term LRT transport of pollutants to the AV and not just the infrequent large-impact LRT events). We used satellite-derived data to identify regional-scale transboundary events and 435 evaluate the effects on $PM_{2.5}$ concentration increments and composition.

    Similar to other studies, thresholds were set for identifying events (Ridley et al., 2012; Carn et al., 2008); however, their selection in this study was representative of local events rather than high-polluted sporadic events. The OM-AOD threshold for BB-LRT events (0.2) agrees with previous results (0.2-0.3) (Kaiser et al., 2012; Misra et al., 2020). The Du-AOD (0.02) threshold was lower (i.e., 0.05) than suggested by Ridley et al. (2012) and that used by Achilleos et al. (2020) to track outstand-440 ing episodes but is of a comparable order of magnitude. In contrast, the $TCSO_2$ threshold in this study for volcanic degassing events differed from that discussed in the literature. The threshold used (0.87 mg/m^2) was lower more than ten times than the used for another degassing volcano (17.15 mg/m^2) (Carn et al., 2008).

    The lower $TCSO_2$ threshold derived in this study is likely linked to the CAMS product we used. While we use the CAMS reanalyses for OM-AOD, Dust-AOD, and $TCSO_2$ for consistency (i.e., tracers from the same model), the representation of 445 the actual magnitude of $TCSO_2$ in the reanalysis product is lower than the operational product. The reanalysis uses an older climatological (2005-2010) emissions dataset (CAMS-GLOB-VOLC) for volcanic degassing (Granier et al., 2019) and only assimilates satellite AOD. While satellite AOD is a useful product to help represent volcanic properties (e.g., volcanic plumes, SO2 concentrations), the operational product also assimilates satellite $TCSO_2$ (CAMS, 2023), providing more constraint on the absolute magnitude of $TCSO_2$. However, regarding this study, the identification process is more important based on the 450 data variability rather than the overall magnitude.

    The identified BB-LRT reproduced the seasonality described in the literature (Mendez-Espinosa et al., 2019; Hernandez et al., 2019; Rodríguez-Gómez et al., 2022). Peak $PM_{2.5}$ concentrations occurred in February and March for BB-LRT events. In concordance with Mendez-Espinosa et al. (2019) and Henao et al. (2021), our findings show that the average conditions in this period are characterized by wind transport from the northeast of the valley, covering part of the Orinoco and Caribbean

455 regions. BB aerosols from fires in the Orinoco can reach the valley through two passes in the Andes mountain range. The limited transport throughout this complex topography might promote the longer stance and accumulation of aerosols, increasing their concentration in the AV (Ballesteros González, 2021). Furthermore, the back-trajectories warn about the Middle Magdalena Valley, which suggests high BB emissions according to the average and the hotspots of OM-AOD. This area has been previously considered critical for open fires in Colombia (Bolaño-Díaz et al., 2022; Ballesteros González, 2021). According to

460 Ballesteros González (2021), fires from this zone are more likely to affect the Andean cities than fires from the Orinoco due to the mountain barriers.

The meteorology characterization for BB-LRT showed some conditions that might enhance the longer influence of the identified events. The assessment highlights the dry conditions in NSA as promoters of both the occurrence of fires and LRT of pollutants. In contrast, despite the high emissions of Amazon fire smoke in the southern hemisphere, these do not considerably

465 increase aerosols in the city due to the scavenging of particles in their transport (Hamburger et al., 2013). The BB-LRT around August might be related to fires in that region (SIATA, 2021; Hamburger et al., 2013).

The estimated contribution to PM$_{2.5}$ concentrations during the BB-LRT showed the highest magnitude for the studied events, with 11.14 $\mu g/m^3$ (37.6%). According to Ballesteros-González et al. (2020), the contribution from BB was calculated to be 4.7 $\mu g/m^3$ for the monitored city in February 2010 and 2018. This finding is consistent with an average (maximum) estimation of

470 6.0 (12.5) $\mu g/m^3$ for samples taken in the same month in 2020. Furthermore, the PMF results support the record of historical events, such as March 2020 at the beginning of the COVID-19 pandemic. For this event, the PMF estimates a maximum contribution of 50.0 $\mu g/m^3$ out of 60.9 $\mu g/m^3$. The particular event was characterized by local emissions suddenly decreasing and climbing in PM$_{2.5}$ concentration (Henao et al., 2021; Mendez-Espinosa et al., 2020).

Like BB-LRT, the monthly frequency of Dust-LRT events coincides with the annual cycle described by other studies. South

475 America experiences a dust reception from the Sahara desert mainly in two trimesters, from March to May and June to August (Prospero et al., 2020). The seasonality of dust events partially coincides with the months of occurrence of BB-LRT events, causing high overlapping between the identified days for these two types of events. Consequently, the identified weak impact on PM$_{2.5}$ by dust events controlled by Andes Mountain (Prospero et al., 2020) might be overshadowed by the most critical effect of BB-LRT. The only widely recognized event recorded for the study period occurred on June 24 and 25, 2020 (Mendez-

480 Espinosa et al., 2020; SIATA, 2021). According to the PMF results, this exhibited almost two times higher contribution to PM$_{2.5}$ than the average event considered in this study. However, the PMF identified equivalent contributions in February 2020. The overlapping between these events might provoke impurities in the PMF factor related to Sahara dust. However, the dust profile aligns with the literature; the organic carbon contribution evidenced a likely mix with a combustion source.

In contrast to BB-LRT and Dust-LRT events, the impact of Volcanic-LRT is expected to be primarily determined by the

485 direction of the wind rather than an actual seasonality in the emissions. Volcanic-LRT events occurred more frequently from July to September, when low to mid-level winds blew from the Nevado del Ruíz volcano region in the southeast, facilitating the transport of emitted aerosols to the AV. According to the sulfur dioxide (SO$_2$) V2 catalog, available on https://so2.gsfc.nasa.gov/measures.html (Fioletov et al., 2023), the AV belongs to the influence area of the Nevado del Ruíz volcano. Indeed, this study identified a significant increment in PM$_{2.5}$ concentrations. According to the PMF results, on average, the contribution for

490 PM$_{2.5}$ was 6.46 μgm^{-3}. Likewise, Casallas et al. (2024) linked the increase in PM$_{2.5}$ concentration during the JJA trimester with volcano activity in Cali, a relatively equidistant city located south of the volcano.

Although the Volcanic-LRT profile is predominantly made by SO$_4^{2-}$, the total concentration of the elements does not show a significant increment compared with surrounding days. This lack of significance in SO$_4^{2-}$ has been observed in other cities where urban sources of SO$_2$ dominated (Miyakawa et al., 2007). However, some alternative hypotheses highlight regarding

495 the magmatic gas state, pointing out that temperature before emissions might provoke low S oxidation and moderate SO$_4^{2-}$ formation (Mather et al., 2003) since SO$_4^{2-}$ precursor formed at high temperature frequently close to the vent (Roberts et al., 2018). For instance, as evidenced in the Volcanic-LRT profile, Cl-poor plumes might reduce S oxidation and forward SO$_4^{2-}$ (Mather et al., 2003).

The results have several implications for future research in the region. Modeling studies in the AV have only considered local

500 emissions as inputs (e.g., Henao et al., 2020; Hernández et al., 2022), and it has been highlighted the need to include external pollution sources as input in chemical transport models to have a more complete representation of air quality in the city. Further, this study suggests conducting shorter chemical campaigns and human health impact studies for target elements and sources, especially in the valley and upwind. For instance, special attention to the carbonaceous matter, F$^-$ and Cd emitted from BB in open fires is needed for human and ecosystem health studies in Colombia (Tuomisto et al., 2008; Jayarathne et al., 2014), since

505 this source is particularly important for the region. The infrequent contribution to Sahara dust is still significant, and there is particular interest in the northern part of the country, where Sahara's most intense events significantly increase the mortality relative risk (Arregocés et al., 2023). On the other hand, Colombia has 12 active volcanoes, highlighting the importance of degassing activity in the country. Monitoring emissions and human health exposure is a primary need for municipalities, especially those close to active volcanoes such as Nevado del Ruíz. Both BB and Volcanic event contribution to heavy metals

510 raise alerts around possible body metal accumulation and diseases such as thyroid cancer (Malandrino et al., 2020; Vigneri et al., 2017). The inhalation intake of these heavy metals sums up to other exposures, such as ingestion and dermal route, which might also be higher near the source (e.g., from water and crop pollution). The increment in Mn and Cr might provoke PM$_{2.5}$ toxicity in lung epithelial cells (Yuan et al., 2019). A deep assessment of the Cr(VI) and Cr(III) needs to be done to evaluate the correct toxicity status of Cr.

515 Finally, this study advertises the need for cooperation among local, national, and international entities to manage complex aerosol sources and human exposure.

5 Conclusions

This study evaluates the impact of BB-LRT, Dust-LRT, and Volcanic-LRT aerosols in the PM$_{2.5}$ concentration and chemical composition in the AV, a densely populated and mountainous region in the tropical Andes. Events for each aerosol type were

520 identified using data with different anomalies from CAMS reanalysis products. Meteorological data from ERA5 and GPM, along with a back-trajectories analysis, were used to link the aerosol events in the AV with the sources and to characterize the meteorological patterns that determine the LRT of aerosols. The impact of these regional events on the local PM$_{2.5}$ was finally

evaluated with local concentration comparisons and characterized through PMF modeling. This study used a unique PM$_{2.5}$ composition campaign from April 2019 to October 2020.

525   The methodology allowed for identifying periods with LRT of pollutants, separating the days before, during, and after the events. During event days, the back-trajectories of air masses arrive from zones previously reported as critical sources of aerosols in the region. This enables the connection between aerosol events in the AV and the sources. The sources were identified as regional fires for BB-LRT, Saharan sands for Dust-LRT, and emissions from the Nevado del Ruíz volcano for volcanic-LRT. The different types of events showed a very marked annual variability. BB-LRT events occurred mainly in

530   February, March, and April, with a lower occurrence during August. Dust-LRT events showed a higher incidence from April to August. Volcanic-LRT showed a high occurrence at the beginning of the second semester (from June to September) and during January and February. No events were identified during October, November, and December.

The weather patterns for BB-LRT events exhibited anomalous low-level northeasterly winds, favoring regional transport of aerosols. Additionally, drier conditions in northern Colombia and Venezuela promoted the occurrence and spread of fires in

535   these regions. For Dust-LRT, more intense winds from the Caribbean at medium levels favor transport to the AV when the aerosol load is high. Moreover, during Volcanic-LRT events, anomalous southeasterly winds at low and medium levels were present, along with low precipitation in the southeast of the AV, where the Nevado del Ruíz volcano is located, enabling the transport to the AV.

When evaluating the impact of LRT events on ground-level PM$_{2.5}$, BB-LRT events resulted in more significant increases

540   in concentrations. The relative increment on PM$_{2.5}$ from Dust-LRT and Volcanic-LRT events was smaller but still significant. Similarly, underpinned by literature-supported profiles, the PMF results evidenced the event's influence on the PM$_{2.5}$ chemical composition. OC species such as OC1 and OC2, anions as F$^-$ and the traces of secondary pollutants SO_4^{2-} and NO$_3^-$ primarily determine the profile identification for BB-LRT. On the other hand, general crustal minerals, together with Ca and Ti, define the Sahara-influenced Dust-LRT profile. Regarding Volcanic-LRT, SO$_4^{2-}$ and characteristic minerals Na, Al, Ca, Fe, Si, K, and

545   Mg represented the profile. Further comparison in positive contributed event days supports the PMF results although identified no substantial SO$_4^{2-}$ rise during volcanic degassing events. This aligned with the observed low Cl$^-$ contribution, supporting the reduced S oxidation hypothesis and forward production of SO$_4^{2-}$. Carbon and ion identification increments were mainly observed for BB-LRT and Volcanic-LRT. Lastly, the profile associated with significant increment in the heavy metals Cr, Mn, Cd and Ni raises concerns. Future studies using chemical models and more detailed measurement and characterization

550   techniques may offer further explanations for this increment.

The findings have several implications for future research. For instance, modeling studies in the region have only considered local emissions as inputs, and external pollution sources, especially volcanic degassing, need to be included as inputs in chemical transport models.

Code availability. A Python code for calculating the back-trajectories is available at https://github.com/MariaPa96/Basic_Trajectories_

555   python.

References

Achilleos, S., Mouzourides, P., Kalivitis, N., Katra, I., Kloog, I., Kouis, P., Middleton, N., Mihalopoulos, N., Neophytou, M., Panayiotou, A., Papatheodorou, S., Savvides, C., Tymvios, F., Vasiliadou, E., Yiallouros, P., and Koutrakis, P.: Spatio-temporal variability of desert dust storms in Eastern Mediterranean (Crete, Cyprus, Israel) between 2006 and 2017 using a uniform methodology, Science of The Total Environment, 714, 136 693, https://doi.org/https://doi.org/10.1016/j.scitotenv.2020.136693, 2020.

Allajbeu, S., Qarri, F., Marku, E., Bekteshi, L., Ibro, V., Frontasyeva, M. V., Stafilov, T., and Lazo, P.: Contamination scale of atmospheric deposition for assessing air quality in Albania evaluated from most toxic heavy metal and moss biomonitoring, Air Quality, Atmosphere & Health, 10, 587–599, https://doi.org/https://doi.org/10.1007/s11869-016-0453-9, 2017.

Andreae, M. O., Andreae, T. W., Annegarn, H., Beer, J., Cachier, H., Le Canut, P., Elbert, W., Maenhaut, W., Salma, I., Wienhold, F. G., and Zenker, T.: Airborne studies of aerosol emissions from savanna fires in southern Africa: 2. Aerosol chemical composition, Journal of Geophysical Research: Atmospheres, 103, 32 119–32 128, https://doi.org/https://doi.org/10.1029/98JD02280, 1998.

Arregocés, H. A., Rojano, R., and Restrepo, G.: Health risk assessment for particulate matter: application of AirQ+ model in the northern Caribbean region of Colombia, Air Quality, Atmosphere & Health, pp. 1–16, 2023.

Aymoz, G., Jaffrezo, J.-L., Jacob, V., Colomb, A., and George, C.: Evolution of organic and inorganic components of aerosol during a Saharan dust episode observed in the French Alps, Atmospheric Chemistry and Physics, 4, 2499–2512, https://doi.org/10.5194/acp-4-2499-2004, 2004.

Ballesteros González, K.: Assessing the effects of medium-range transport of biomass burning aerosols on air quality in Northern South America through chemical transport modelling, Ph.D. thesis, 2021.

Ballesteros-González, K., Sullivan, A. P., and Morales-Betancourt, R.: Estimating the air quality and health impacts of biomass burning in northern South America using a chemical transport model, Science of The Total Environment, 739, 139 755, https://doi.org/https://doi.org/10.1016/j.scitotenv.2020.139755, 2020.

Bedoya, A., Nisperuza, D., Alegría, D., Múnera, M., Guerrero-Rascado, J. L., Zapata, C. E., Jiménez, J. F., Landulfo, E., and Bastidas, Á.: Strong Saharan Dust Event Detected at Lalinet LOA-UNAL Station, over Medellín, Colombia by Active and Passive Remote Sensing, 119, 08 006, https://doi.org/https://doi.org/10.1051/epjconf/201611908006, 2016.

Bia, G., Borgnino, L., Zampieri, G., and Garcia, M.: Fluorine surface speciation in South Andean volcanic ashes, Chemical Geology, 532, 119 402, https://doi.org/https://doi.org/10.1016/j.chemgeo.2019.119402, 2020.

Bolaño-Díaz, S., Camargo-Caicedo, Y., Soro, T. D., N'Dri, A. B., and Bolaño-Ortiz, T. R.: Spatio-Temporal Characterization of Fire Using MODIS Data (2000ndash;2020) in Colombia, Fire, 5, https://doi.org/10.3390/fire5050134, 2022.

Bolaño-Ortiz, T. R., Constante-Ballestas, J. I., Puliafito, S. E., Vélez-Pereira, A. M., Tovar-Bernal, F. A., and Camargo-Caicedo, Y.: Spread COVID-19 during Godzilla African dust in June 2020 on the Colombian Caribbean region, Atmospheric Pollution Research, 14, 101 860, https://doi.org/https://doi.org/10.1016/j.apr.2023.101860, 2023a.

Bolaño-Ortiz, T. R., Díaz-Gutiérrez, V. L., Vélez-Pereira, A. M., Vergara-Vásquez, E. L., and Camargo-Caicedo, Y.: Snow Albedo Reduction in the Colombian Andes Mountains Due to 2000 to 2020 Saharan Dust Intrusions Events, Water, 15, https://doi.org/10.3390/w15173150, 2023b.

Boyd, P. W. and Ellwood, M. J.: The biogeochemical cycle of iron in the ocean, Nature Geoscience, 3, 675–682, https://doi.org/https://doi.org/10.1038/ngeo964, 2010.

Briffa, J., Sinagra, E., and Blundell, R.: Heavy metal pollution in the environment and their toxicological effects on humans, Heliyon, 6, e04 691, https://doi.org/https://doi.org/10.1016/j.heliyon.2020.e04691, 2020.

Callén, M., de la Cruz, M., López, J., Navarro, M., and Mastral, A.: Comparison of receptor models for source apportionment of the PM10 in Zaragoza (Spain), Chemosphere, 76, 1120–1129, https://doi.org/https://doi.org/10.1016/j.chemosphere.2009.04.015, 2009.

CAMS: Global atmospheric composition forecast data documentation, https://confluence.ecmwf.int/display/CKB/CAMS%3A+Global+ atmospheric+composition+forecast+data+documentation#heading-Satelliteobservations, 2023.

Carn, S., Krueger, A., Arellano, S., Krotkov, N., and Yang, K.: Daily monitoring of Ecuadorian volcanic degassing from space, Journal of Volcanology and Geothermal Research, 176, 141–150, https://doi.org/https://doi.org/10.1016/j.jvolgeores.2008.01.029, recent and active volcanism in the Ecuadorian Andes, 2008.

Carn, S., Clarisse, L., and Prata, A.: Multi-decadal satellite measurements of global volcanic degassing, Journal of Volcanology and Geothermal Research, 311, 99–134, https://doi.org/https://doi.org/10.1016/j.jvolgeores.2016.01.002, 2016.

Casallas, A., Castillo-Camacho, M. P., Guevara-Luna, M. A., González, Y., Sanchez, E., and Belalcazar, L. C.: Spatio-temporal analysis of PM2.5 and policies in Northwestern South America, Science of The Total Environment, 852, 158 504, https://doi.org/https://doi.org/10.1016/j.scitotenv.2022.158504, 2022.

Casallas, A., Cabrera, A., Guevara-Luna, M.-A., Tompkins, A., González, Y., Aranda, J., Belalcazar, L. C., Mogollon-Sotelo, C., Celis, N., Lopez-Barrera, E., Peña-Rincon, C. A., and Ferro, C.: Air pollution analysis in Northwestern South America: A new Lagrangian framework, Science of The Total Environment, 906, 167 350, https://doi.org/https://doi.org/10.1016/j.scitotenv.2023.167350, 2024.

Choobari, O. A., Zawar-Reza, P., and Sturman, A.: The global distribution of mineral dust and its impacts on the climate system: A review, Atmospheric Research, 138, 152–165, https://doi.org/https://doi.org/10.1016/j.atmosres.2013.11.007, 2014.

Chow, J. C., Watson, J. G., Kuhns, H., Etyemezian, V., Lowenthal, D. H., Crow, D., Kohl, S. D., Engelbrecht, J. P., and Green, M. C.: Source profiles for industrial, mobile, and area sources in the Big Bend Regional Aerosol Visibility and Observational study, Chemosphere, 54, 185–208, https://doi.org/https://doi.org/10.1016/j.chemosphere.2003.07.004, 2004.

Corrales Espinosa, A., García, J., and Posada, C.: congestión vehicular en medellin una posible solución desde la economía, https://doi.org/10.13140/RG.2.2.28140.36480, 2016.

Cuesta-Mosquera, A. P., Wahl, M., Acosta-López, J. G., García-Reynoso, J. A., and Aristizábal-Zuluaga, B. H.: Mixing layer height and slope wind oscillation: Factors that control ambient air SO2 in a tropical mountain city, Sustainable Cities and Society, 52, 101 852, https://doi.org/https://doi.org/10.1016/j.scs.2019.101852, 2020.

Delmelle, P., Maters, E. C., Calkins, J. A., Gaspard, F., Opfergelt, S., and Jenkins, S. F.: Eruptive style controls the formation of silicon hexafluoride salts on volcanic ash: The case of the 2010 eruption of Eyjafjallajökull volcano, Iceland, Chemical Geology, 579, 120 327, https://doi.org/https://doi.org/10.1016/j.chemgeo.2021.120327, 2021.

Dong, X., Fu, J. S., Zhu, Q., Sun, J., Tan, J., Keating, T., Sekiya, T., Sudo, K., Emmons, L., Tilmes, S., Jonson, J. E., Schulz, M., Bian, H., Chin, M., Davila, Y., Henze, D., Takemura, T., Benedictow, A. M. K., and Huang, K.: Long-range transport impacts on surface aerosol concentrations and the contributions to haze events in China: an HTAP2 multi-model study, Atmospheric Chemistry and Physics, 18, 15 581–15 600, https://doi.org/10.5194/acp-18-15581-2018, 2018.

Echeverri, A. and Orsini, F.: Informalidad y urbanismo social en Medellín, https://www.eafit.edu.co/centros/urbam/articulos-publicaciones/ Documents/111103_RS3_AEcheverri_%20P%2011-24.pdf, 2011.

Eugene Kim, P. K. H. and Edgerton, E. S.: Source Identification of Atlanta Aerosol by Positive Matrix Factorization, Journal of the Air & Waste Management Association, 53, 731–739, https://doi.org/10.1080/10473289.2003.10466209, 2003.

655   Eugene Kim, P. K. H. and Qin, Y.: Estimation of Organic Carbon Blank Values and Error Structures of the Speciation Trends Network Data for Source Apportionment, Journal of the Air & Waste Management Association, 55, 1190–1199, https://doi.org/10.1080/10473289.2005.10464705, 2005.

European Commision: EU air quality standards, https://environment.ec.europa.eu/topics/air/air-quality/eu-air-quality-standards_en, 2019.

Fioletov, V. E., McLinden, C. A., Krotkov, N., Li, C., Joiner, J., Theys, N., Carn, S., and Moran, M. D.: A global catalogue of large
660   SO 2 sources and emissions derived from the Ozone Monitoring Instrument, Atmospheric Chemistry and Physics, 16, 11 497–11 519, https://doi.org/https://doi.org/10.5194/acp-16-11497-2016, 2016.

Fioletov, V. E., McLinden, C. A., Griffin, D., Abboud, I., Krotkov, N., Leonard, P. J. T., Li, C., Joiner, J., Theys, N., and Carn, S.: Version 2 of the global catalogue of large anthropogenic and volcanic SO_2 sources and emissions derived from satellite measurements, Earth System Science Data, 15, 75–93, https://doi.org/10.5194/essd-15-75-2023, 2023.

665   Granier, C., Darras, S., van Der Gon, H. D., Jana, D., Elguindi, N., Bo, G., Michael, G., Marc, G., Jalkanen, J.-P., Kuenen, J., et al.: The Copernicus atmosphere monitoring service global and regional emissions (April 2019 version), https://doi.org/doi:10.24380/d0bn-kx16, 2019.

Gómez-Marín, M., Yepes, D. L., Patiño, K., Grajales, D., Tavera, J., and Vergara-Correa, J. A.: Convenio interadministrativo 671 de 2021. AMVA-PCJIC, https://www.metropol.gov.co/ambiental/calidad-del-aire/Biblioteca-aire/Estudios-calidad-del-aire/
670   Informe-Final-Caracterizacion-Fase-IV.pdf, 2021.

Gómez Peláez, L. M., Santos, J. M., de Almeida Albuquerque, T. T., Reis, N. C., Andreão, W. L., and de Fátima Andrade, M.: Air quality status and trends over large cities in South America, Environmental Science Policy, 114, 422–435, https://doi.org/https://doi.org/10.1016/j.envsci.2020.09.009, 2020.

Hamburger, T., Matisāns, M., Tunved, P., Ström, J., Calderon, S., Hoffmann, P., Hochschild, G., Gross, J., Schmeissner, T., Wiedensohler, A.,
675   and Krejci, R.: Long-term in situ observations of biomass burning aerosol at a high altitude station in Venezuela ndash; sources, impacts and interannual variability, Atmospheric Chemistry and Physics, 13, 9837–9853, https://doi.org/10.5194/acp-13-9837-2013, 2013.

Henao, J. J., Mejía, J. F., Rendón, A. M., and Salazar, J. F.: Sub-kilometer dispersion simulation of a CO tracer for an inter-Andean urban valley, Atmospheric Pollution Research, 11, 928–945, https://doi.org/https://doi.org/10.1016/j.apr.2020.02.005, 2020.

Henao, J. J., Rendón, A. M., Hernández, K. S., Giraldo-Ramirez, P. A., Robledo, V., Posada-Marín, J. A., Bernal, N., Salazar, J. F., and
680   Mejía, J. F.: Differential Effects of the COVID-19 Lockdown and Regional Fire on the Air Quality of Medellín, Colombia, Atmosphere, 12, https://doi.org/10.3390/atmos12091137, 2021.

Hernandez, A. J., Morales-Rincon, L. A., Wu, D., Mallia, D., Lin, J. C., and Jimenez, R.: Transboundary transport of biomass burning aerosols and photochemical pollution in the Orinoco River Basin, Atmospheric Environment, 205, 1–8, https://doi.org/https://doi.org/10.1016/j.atmosenv.2019.01.051, 2019.

685   Hernández, K. S., Henao, J. J., and Rendón, A. M.: Dispersion simulations in an Andean city: Role of continuous traffic data in the spatio-temporal distribution of traffic emissions, Atmospheric Pollution Research, 13, 101 361, https://doi.org/https://doi.org/10.1016/j.apr.2022.101361, 2022.

Herrera-Mejía, L. and Hoyos, C. D.: Characterization of the atmospheric boundary layer in a narrow tropical valley using remote-sensing and radiosonde observations and the WRF model: the Aburrá Valley case-study, Quarterly Journal of the Royal Meteorological Society,
690   145, 2641–2665, https://doi.org/https://doi.org/10.1002/qj.3583, 2019.

Hersbach, H., Bell, B., Berrisford, P., Hirahara, S., Horányi, A., Muñoz-Sabater, J., Nicolas, J., Peubey, C., Radu, R., Schepers, D., et al.: The ERA5 global reanalysis, Quarterly Journal of the Royal Meteorological Society, 146, 1999–2049, 2020.

Huffman, G., Stocker, E., Bolvin, D., Nelkin, E., and Tan, J.: GPM IMERG Final Precipitation L3 1 day 0.1 degree x 0.1 degree V06, Edited by Andrey Savtchenko, Greenbelt, MD, Goddard Earth Sciences Data and Information Services Center (GES DISC), https://doi.org/10.5067/GPM/IMERGDF/DAY/06, 2019.

695

Huntzicker, J. J., Heyerdahl, E. K., McDow, S. R., Rau, J. A., Griest, W. H., and MacDougall, C. S.: Combustion as the Principal Source of Carbonaceous Aerosol in the Ohio River Valley, Journal of the Air Pollution Control Association, 36, 705–709, https://doi.org/10.1080/00022470.1986.10466105, 1986.

Hwang, S.-H., Lee, J. Y., Yi, S.-M., and Kim, H.: Associations of particulate matter and its components with emergency room visits for cardiovascular and respiratory diseases, PLoS One, 12, e0183 224, https://doi.org/https://doi.org/10.1371/journal.pone.0183224, 2017.

700

Inness, A., Ades, M., Agustí-Panareda, A., Barré, J., Benedictow, A., Blechschmidt, A.-M., Dominguez, J. J., Engelen, R., Eskes, H., Flemming, J., Huijnen, V., Jones, L., Kipling, Z., Massart, S., Parrington, M., Peuch, V.-H., Razinger, M., Remy, S., Schulz, M., and Suttie, M.: The CAMS reanalysis of atmospheric composition, Atmospheric Chemistry and Physics, 19, 3515–3556, https://doi.org/10.5194/acp-19-3515-2019, 2019.

705

Jayarathne, T., Stockwell, C. E., Yokelson, R. J., Nakao, S., and Stone, E. A.: Emissions of Fine Particle Fluoride from Biomass Burning, Environmental Science & Technology, 48, 12 636–12 644, https://doi.org/10.1021/es502933j, pMID: 25275955, 2014.

Jiao, Y., Su, M., Ji, C., Yang, S., and Zhang, P.: How to design fully cooperative policies to abate transboundary air pollution between two highly asymmetric regions: An abnormal incrementalism analysis, Journal of Cleaner Production, 278, 124 042, https://doi.org/https://doi.org/10.1016/j.jclepro.2020.124042, 2021.

710

Kaiser, J. W., Heil, A., Andreae, M. O., Benedetti, A., Chubarova, N., Jones, L., Morcrette, J.-J., Razinger, M., Schultz, M. G., Suttie, M., and van der Werf, G. R.: Biomass burning emissions estimated with a global fire assimilation system based on observed fire radiative power, Biogeosciences, 9, 527–554, https://doi.org/10.5194/bg-9-527-2012, 2012.

Kaneyasu, N., Yamamoto, S., Sato, K., Takami, A., Hayashi, M., Hara, K., Kawamoto, K., Okuda, T., and Hatakeyama, S.: Impact of long-range transport of aerosols on the PM2.5 composition at a major metropolitan area in the northern Kyushu area of Japan, Atmospheric

715

Environment, 97, 416–425, https://doi.org/https://doi.org/10.1016/j.atmosenv.2014.01.029, 2014.

Kaspari, S., Painter, T. H., Gysel, M., Skiles, S. M., and Schwikowski, M.: Seasonal and elevational variations of black carbon and dust in snow and ice in the Solu-Khumbu, Nepal and estimated radiative forcings, Atmospheric Chemistry and Physics, 14, 8089–8103, https://doi.org/10.5194/acp-14-8089-2014, 2014.

Kulshrestha, U., Kumar, B., et al.: Airmass trajectories and long range transport of pollutants: review of wet deposition scenario in South

720

Asia, Advances in Meteorology, 2014, https://doi.org/https://doi.org/10.1155/2014/596041, 2014.

Kumar, A., Abouchami, W., Galer, S., Garrison, V., Williams, E., and Andreae, M.: A radiogenic isotope tracer study of transatlantic dust transport from Africa to the Caribbean, Atmospheric Environment, 82, 130–143, https://doi.org/https://doi.org/10.1016/j.atmosenv.2013.10.021, 2014.

Liang, C.-K., West, J. J., Silva, R. A., Bian, H., Chin, M., Davila, Y., Dentener, F. J., Emmons, L., Flemming, J., Folberth, G., Henze, D., Im,

725

U., Jonson, J. E., Keating, T. J., Kucsera, T., Lenzen, A., Lin, M., Lund, M. T., Pan, X., Park, R. J., Pierce, R. B., Sekiya, T., Sudo, K., and Takemura, T.: HTAP2 multi-model estimates of premature human mortality due to intercontinental transport of air pollution and emission sectors, Atmospheric Chemistry and Physics, 18, 10 497–10 520, https://doi.org/10.5194/acp-18-10497-2018, 2018.

Lin, P., Hu, M., Deng, Z., Slanina, J., Han, S., Kondo, Y., Takegawa, N., Miyazaki, Y., Zhao, Y., and Sugimoto, N.: Seasonal and diurnal variations of organic carbon in PM2.5 in Beijing and the estimation of secondary organic carbon, Journal of Geophysical Research:

730

Atmospheres, 114, https://doi.org/https://doi.org/10.1029/2008JD010902, 2009.

Lippmann, M., Chen, L.-C., Gordon, T., Ito, K., and Thurston, G. D.: National Particle Component Toxicity (NPACT) Initiative: integrated epidemiologic and toxicologic studies of the health effects of particulate matter components, Research report (Health Effects Institute), p. 5—13, http://europepmc.org/abstract/MED/24377209, 2013.

Liu, J., Li, J., and Yao, F.: Source-receptor relationship of transboundary particulate matter pollution between China, South Korea and Japan: Approaches, current understanding and limitations, Critical Reviews in Environmental Science and Technology, 52, 3896–3920, https://doi.org/10.1080/10643389.2021.1964308, 2022.

Malaguti, A., Mircea, M., La Torretta, T. M., Telloli, C., Petralia, E., Stracquadanio, M., and Berico, M.: Chemical Composition of Fine and Coarse Aerosol Particles in the Central Mediterranean Area during Dust and Non-Dust Conditions, Aerosol and Air Quality Research, 15, 410–425, https://doi.org/10.4209/aaqr.2014.08.0172, 2015.

Malandrino, P., Russo, M., Gianì, F., Pellegriti, G., Vigneri, P., Belfiore, A., Rizzarelli, E., and Vigneri, R.: Increased Thyroid Cancer Incidence in Volcanic Areas: A Role of Increased Heavy Metals in the Environment?, International Journal of Molecular Sciences, 21, https://doi.org/10.3390/ijms21103425, 2020.

Martin, R., Ilyinskaya, E., and Oppenheimer, C.: The enigma of reactive nitrogen in volcanic emissions, Geochimica et Cosmochimica Acta, 95, 93–105, https://doi.org/https://doi.org/10.1016/j.gca.2012.07.027, 2012.

Martinez-Verduzco, R., Reyna-Gomez, L., Cruz-López, A., Carrillo-Avila, J., Valdez-Cavazos, A., and Suárez-Vázquez, S.: Approach into the influence of Saharan dust on the physicochemical properties of PM2. 5 in Monterrey, México, International Journal of Environmental Science and Technology, pp. 1–14, 2023.

Martinsson, B. G., Brenninkmeijer, C. A. M., Carn, S. A., Hermann, M., Heue, K.-P., van Velthoven, P. F. J., and Zahn, A.: Influence of the 2008 Kasatochi volcanic eruption on sulfurous and carbonaceous aerosol constituents in the lower stratosphere, Geophysical Research Letters, 36, https://doi.org/https://doi.org/10.1029/2009GL038735, 2009.

Mason, E., Wieser, P. E., Liu, E. J., Edmonds, M., Ilyinskaya, E., Whitty, R. C., Mather, T. A., Elias, T., Nadeau, P. A., Wilkes, T. C., et al.: Volatile metal emissions from volcanic degassing and lava–seawater interactions at Kīlauea Volcano, Hawai'i, Communications Earth & Environment, 2, 79, 2021.

Mather, T., Pyle, D., and Oppenheimer, C.: Tropospheric volcanic aerosol, Geophysical Monograph-American Geophysical Union, 139, 189–212, 2003.

Mendez Espinosa, J., Herrera, L., and Belalcazar, L.: Study of a Saharan Dust Intrusion into the Colombian Atmosphere/ Estudio de una intrusión de polvo sahariano en la atmósfera de Colombia, Revista Ingenierías Universidad de Medellín, 17, 17–34, https://doi.org/10.22395/rium.v17n32a1, 2018.

Mendez-Espinosa, J., Belalcazar, L., and Betancourt, R. M.: Regional air quality impact of northern South America biomass burning emissions, Atmospheric environment, 203, 131–140, https://doi.org/https://doi.org/10.1016/j.atmosenv.2019.01.042, 2019.

Mendez-Espinosa, J. F., Rojas, N. Y., Vargas, J., Pachón, J. E., Belalcazar, L. C., and Ramírez, O.: Air quality variations in Northern South America during the COVID-19 lockdown, Science of The Total Environment, 749, 141 621, https://doi.org/https://doi.org/10.1016/j.scitotenv.2020.141621, 2020.

Misra, A., Tripathi, S., Sembhi, H., and Boesch, H.: Validation of CAMS AOD using AERONET Data and Trend Analysis at Four Locations in the Indo-Gangetic Basin, Annales Geophysicae Discussions, 2020, 1–25, https://doi.org/10.5194/angeo-2020-40, 2020.

Miyakawa, T., Takegawa, N., and Kondo, Y.: Removal of sulfur dioxide and formation of sulfate aerosol in Tokyo, Journal of Geophysical Research: Atmospheres, 112, https://doi.org/https://doi.org/10.1029/2006JD007896, 2007.

Moran-Zuloaga, D., Merchan-Merchan, W., Rodriguez-Caballero, E., Mulas, M., and Hernick, P.: Long-range transport and microscopy analysis of Sangay volcanic ashes in Ecuador, Air Quality, Atmosphere & Health, pp. 1–21, https://doi.org/https://doi.org/10.1007/s11869-023-01434-w, 2023.

Moreno, C. I., Krejci, R., Jaffrezo, J.-L., Uzu, G., Alastuey, A., Andrade, M. F., Mardóñez, V., Koenig, A. M., Aliaga, D., Mohr, C., Ticona, L., Velarde, F., Blacutt, L., Forno, R., Whiteman, D. N., Wiedensohler, A., Ginot, P., and Laj, P.: Tropical tropospheric aerosol sources and chemical composition observed at high-altitude in the Bolivian Andes, EGUsphere, 2023, 1–39, https://doi.org/10.5194/egusphere-2023-1298, 2023.

Nicolás, J., Chiari, M., Crespo, J., Orellana, I. G., Lucarelli, F., Nava, S., Pastor, C., and Yubero, E.: Quantification of Saharan and local dust impact in an arid Mediterranean area by the positive matrix factorization (PMF) technique, Atmospheric Environment, 42, 8872–8882, https://doi.org/https://doi.org/10.1016/j.atmosenv.2008.09.018, 2008.

Okin, G. S., Mahowald, N., Chadwick, O. A., and Artaxo, P.: Impact of desert dust on the biogeochemistry of phosphorus in terrestrial ecosystems, Global Biogeochemical Cycles, 18, https://doi.org/https://doi.org/10.1029/2003GB002145, 2004.

Paatero, P.: Least squares formulation of robust non-negative factor analysis, Chemometrics and Intelligent Laboratory Systems, 37, 23–35, https://doi.org/https://doi.org/10.1016/S0169-7439(96)00044-5, 1997.

Paatero, P. and Tapper, U.: Positive matrix factorization: A non-negative factor model with optimal utilization of error estimates of data values, Environmetrics, 5, 111–126, 1994.

Pani, S. K., Chantara, S., Khamkaew, C., Lee, C.-T., and Lin, N.-H.: Biomass burning in the northern peninsular Southeast Asia: Aerosol chemical profile and potential exposure, Atmospheric Research, 224, 180–195, https://doi.org/https://doi.org/10.1016/j.atmosres.2019.03.031, 2019.

Pérez-Carrasquilla, J. S., Montoya, P. A., Sánchez, J. M., Hernández, K. S., and Ramírez, M.: Forecasting 24 h averaged $PM_{2.5}$ concentration in the Aburrá Valley using tree-based machine learning models, global forecasts, and satellite information, Advances in Statistical Climatology, Meteorology and Oceanography, 9, 121–135, https://doi.org/10.5194/ascmo-9-121-2023, 2023.

Pongpiachan, S., Tipmanee, D., Choochuay, C., Hattayanone, M., Deelaman, W., Iadtem, N., Bunsomboonsakul, S., Palakun, J., Poshyachinda, S., Leckngam, A., et al.: Vertical profile of organic and elemental carbon in sediments of Songkhla Lake, Thailand, Limnology, 20, 203–214, 2019.

Posada-Marín, J. A., Rendón, A. M., Salazar, J. F., Mejía, J. F., and Villegas, J. C.: WRF downscaling improves ERA-Interim representation of precipitation around a tropical Andean valley during El Niño: implications for GCM-scale simulation of precipitation over complex terrain, Climate Dynamics, 52, 3609–3629, 2019.

Pouliot, G., Pierce, T., Denier van der Gon, H., Schaap, M., Moran, M., and Nopmongcol, U.: Comparing emission inventories and model-ready emission datasets between Europe and North America for the AQMEII project, Atmospheric Environment, 53, 4–14, https://doi.org/https://doi.org/10.1016/j.atmosenv.2011.12.041, aQMEII: An International Initiative for the Evaluation of Regional-Scale Air Quality Models - Phase 1, 2012.

Prospero, J. M., Collard, F.-X., Molinié, J., and Jeannot, A.: Characterizing the annual cycle of African dust transport to the Caribbean Basin and South America and its impact on the environment and air quality, Global Biogeochemical Cycles, 28, 757–773, https://doi.org/https://doi.org/10.1002/2013GB004802, 2014.

Prospero, J. M., Barkley, A. E., Gaston, C. J., Gatineau, A., Campos y Sansano, A., and Panechou, K.: Characterizing and quantifying African dust transport and deposition to South America: Implications for the phosphorus budget in the Amazon Basin, Global Biogeochemical Cycles, 34, e2020GB006 536, 2020.

Rastogi, N., Singh, A., Singh, D., and Sarin, M.: Chemical characteristics of PM2.5 at a source region of biomass burning emissions: Evidence for secondary aerosol formation, Environmental Pollution, 184, 563–569, https://doi.org/https://doi.org/10.1016/j.envpol.2013.09.037, 2014.

Ridley, D. A., Heald, C. L., and Ford, B.: North African dust export and deposition: A satellite and model perspective, Journal of Geophysical Research: Atmospheres, 117, https://doi.org/https://doi.org/10.1029/2011JD016794, 2012.

Roberts, T., Vignelles, D., Liuzzo, M., Giudice, G., Aiuppa, A., Coltelli, M., Salerno, G., Chartier, M., Couté, B., Berthet, G., Lurton, T., Dulac, F., and Renard, J.-B.: The primary volcanic aerosol emission from Mt Etna: Size-resolved particles with SO2 and role in plume reactive halogen chemistry, Geochimica et Cosmochimica Acta, 222, 74–93, https://doi.org/https://doi.org/10.1016/j.gca.2017.09.040, 2018.

Rodríguez-Gómez, C., Echeverry, G., Jaramillo, A., and Ladino, L. A.: The negative impact of biomass burning and the Orinoco low-level jet on the air quality of the Orinoco River Basin, Atmósfera, https://doi.org/https://doi.org/10.20937/ATM.52979, 2022.

Ruggieri, F., Fernandez-Turiel, J., Saavedra, J., Gimeno, D., Polanco, E., Amigo, A., Galindo, G., and Caselli, A.: Contribution of volcanic ashes to the regional geochemical balance: The 2008 eruption of Chaitén volcano, Southern Chile, Science of The Total Environment, 425, 75–88, https://doi.org/https://doi.org/10.1016/j.scitotenv.2012.03.011, 2012.

Salazar Hernandez, C., Vásquez, J., and Agudelo, N.: Perspectiva paisajística de la estructura ecológica urbana de Medellín, ISBN 9786285000812, https://doi.org/10.18566/978-628-500-081-2, 2022.

Salim, I., Sajjad, R. U., Paule-Mercado, M. C., Memon, S. A., Lee, B.-Y., Sukhbaatar, C., and Lee, C.-H.: Comparison of two receptor models PCA-MLR and PMF for source identification and apportionment of pollution carried by runoff from catchment and sub-watershed areas with mixed land cover in South Korea, Science of The Total Environment, 663, 764–775, https://doi.org/https://doi.org/10.1016/j.scitotenv.2019.01.377, 2019.

Santín, C., Doerr, S. H., Kane, E. S., Masiello, C. A., Ohlson, M., de la Rosa, J. M., Preston, C. M., and Dittmar, T.: Towards a global assessment of pyrogenic carbon from vegetation fires, Global Change Biology, 22, 76–91, https://doi.org/https://doi.org/10.1111/gcb.12985, 2016.

Satsumabayashi, H., Kawamura, M., Katsuno, T., Futaki, K., Murano, K., Carmichael, G. R., Kajino, M., Horiguchi, M., and Ueda, H.: Effects of Miyake volcanic effluents on airborne particles and precipitation in central Japan, Journal of Geophysical Research: Atmospheres, 109, https://doi.org/https://doi.org/10.1029/2003JD004204, 2004.

Shin, S. M., Kim, J. Y., Lee, J. Y., Kim, D.-S., and Kim, Y. P.: Enhancement of modeling performance by including organic markers to the PMF modeling for the PM2. 5 at Seoul, Air Quality, Atmosphere & Health, 15, 91–104, https://doi.org/https://doi.org/10.1007/s11869-021-01087-7, 2022.

SIATA: Seguimiento de los aerosoles y eventos externos que afectan la calidad del aire del Valle de Aburrá, https://www.metropol.gov.co/ambiental/calidad-del-aire/Biblioteca-aire/Estudios-calidad-del-aire/Estudio-Fuentes-Externas-SIATA.pdf, 2021.

Trejos, E. M., Silva, L. F., Hower, J. C., Flores, E. M., González, C. M., Pachón, J. E., and Aristizábal, B. H.: Volcanic emissions and atmospheric pollution: A study of nanoparticles, Geoscience Frontiers, 12, 746–755, 2021.

Tuomisto, J. T., Wilson, A., Evans, J. S., and Tainio, M.: Uncertainty in mortality response to airborne fine particulate matter: Combining European air pollution experts, Reliability Engineering   System Safety, 93, 732–744, https://doi.org/https://doi.org/10.1016/j.ress.2007.03.002, expert Judgement, 2008.

UN: HEMISPHERIC TRANSPORT OF AIR POLLUTION, https://unece.org/sites/default/files/2021-06/Air.Pollution%20Studies.No_.17_100.pdf, 2010.

US-EPA: EPA Positive Matrix Factorization (PMF) 5.0 Fundamentals and User Guide, https://www.epa.gov/sites/production/files/2015-02/documents/pmf_5.0_user_guide.pdf, 2014.

Vanegas, S., Trejos, E. M., Aristizábal, B. H., Pereira, G. M., Hernández, J. M., Murillo, J. H., Ramírez, O., Amato, F., Silva, L. F. O., Rojas, N. Y., Zafra, C., and Pachón, J. E.: Spatial Distribution and Chemical Composition of Road Dust in Two High-Altitude Latin American Cities, Atmosphere, 12, https://doi.org/10.3390/atmos12091109, 2021.

Varrica, D., Tamburo, E., Vultaggio, M., and Di Carlo, I.: ATR–FTIR Spectral Analysis and Soluble Components of PM10 And PM2.5 Particulate Matter over the Urban Area of Palermo (Italy) during Normal Days and Saharan Events, International Journal of Environmental Research and Public Health, 16, https://doi.org/10.3390/ijerph16142507, 2019.

Vigneri, R., Malandrino, P., Gianì, F., Russo, M., and Vigneri, P.: Heavy metals in the volcanic environment and thyroid cancer, Molecular and Cellular Endocrinology, 457, 73–80, https://doi.org/https://doi.org/10.1016/j.mce.2016.10.027, hormone-related cancers and endocrine disruptors: new aspects of an old question, 2017.

Wang, L., Liu, Z., Sun, Y., Ji, D., and Wang, Y.: Long-range transport and regional sources of PM2.5 in Beijing based on long-term observations from 2005 to 2010, Atmospheric Research, 157, 37–48, https://doi.org/https://doi.org/10.1016/j.atmosres.2014.12.003, 2015.

WHO: WHO global air quality guidelines: particulate matter (PM2. 5 and PM10), ozone, nitrogen dioxide, sulfur dioxide and carbon monoxide: executive summary, 2021.

Woo, J.-H., Kim, Y., Kim, H.-K., Choi, K.-C., Eum, J.-H., Lee, J.-B., Lim, J.-H., Kim, J., and Seong, M.: Development of the CREATE Inventory in Support of Integrated Climate and Air Quality Modeling for Asia, Sustainability, 12, https://doi.org/10.3390/su12197930, 2020.

Xie, W., You, J., Zhi, C., and Li, L.: The toxicity of ambient fine particulate matter (PM2.5) to vascular endothelial cells, Journal of Applied Toxicology, 41, 713–723, https://doi.org/https://doi.org/10.1002/jat.4138, 2021.

Yao, L., Huo, J., Wang, D., Fu, Q., Sun, W., Li, Q., and Chen, J.: Online measurement of carbonaceous aerosols in suburban Shanghai during winter over a three-year period: Temporal variations, meteorological effects, and sources, Atmospheric Environment, 226, 117 408, https://doi.org/https://doi.org/10.1016/j.atmosenv.2020.117408, 2020.

Yu, J., Yan, C., Liu, Y., Li, X., Zhou, T., Zheng, M., et al.: Potassium: a tracer for biomass burning in Beijing?, Aerosol and Air Quality Research, 18, 2447–2459, https://doi.org/10.4209/aaqr.2017.11.0536, 2018.

Yuan, Y., Wu, Y., Ge, X., Nie, D., Wang, M., Zhou, H., and Chen, M.: In vitro toxicity evaluation of heavy metals in urban air particulate matter on human lung epithelial cells, Science of The Total Environment, 678, 301–308, https://doi.org/https://doi.org/10.1016/j.scitotenv.2019.04.431, 2019.

Zhao, N., Dong, X., Huang, K., Fu, J. S., Lund, M. T., Sudo, K., Henze, D., Kucsera, T., Lam, Y. F., Chin, M., and Tilmes, S.: Responses of Arctic black carbon and surface temperature to multi-region emission reductions: a Hemispheric Transport of Air Pollution Phase 2 (HTAP2) ensemble modeling study, Atmospheric Chemistry and Physics, 21, 8637–8654, https://doi.org/10.5194/acp-21-8637-2021, 2021.

Zhong, L., Louie, P. K., Zheng, J., Yuan, Z., Yue, D., Ho, J. W., and Lau, A. K.: Science–policy interplay: Air quality management in the Pearl River Delta region and Hong Kong, Atmospheric Environment, 76, 3–10, https://doi.org/https://doi.org/10.1016/j.atmosenv.2013.03.012, improving Regional Air Quality over the Pearl River Delta and Hong Kong: from Science to Policy, 2013.